MNRAS 000, 1–16 (2020) Preprint 24 November 2021 Compiled using MNRAS LATEX style file v3.0

Hyper-Eddington accretion flows onto black holes accompanied by powerful outflows

Eishun Takeo[1]★, Kohei Inayoshi[2,3]†, and Shin Mineshige[1]
[1]Department of Astronomy, Graduate School of Science, Kyoto University, Kitashirakawa, Oiwakecho, Sakyo-ku, Kyoto, 606-8502, Japan
[2]The Kavli Institute for Astronomy and Astrophysics, Peking University, 5 Yiheyuan Road, Haidian District, Beijing 100871, P. R. China
[3]Department of Astronomy, School of Physics, Peking University, Beijing 100871, P. R. China

arXiv:2002.07187v1 [astro-ph.HE] 17 Feb 2020

Accepted XXX. Received YYY; in original form ZZZ

ABSTRACT

We perform two-dimensional radiation hydrodynamical simulations of accretion flows onto black holes (BHs) at the nuclei of protogalaxies, and study the impact of mechanical and radiative feedback on rapid growth of BHs. The outflows deposit mass, momentum and energy into the surrounding medium and prevent mass accretion onto the BH, resulting in the reduction of radiative output. We find that when the BH is embedded in a dense gas core, ionizing radiation attenuated by inefficient BH feeding owing to mechanical feedback hardly affects the gas dynamics at the BH gravitational sphere of influence, from which intense inflows of neutral gas occur at rates substantially exceeding the Eddington limit without impeded by photoionization and heating. Since mechanical power of outflows driven by the rapidly accreting BH is sufficiently strong, bipolar outflows completely evacuate the surrounding gas in the polar region but mass inflows through the equatorial region maintain the BH accretion rate as high as $\sim 300-10^3\ \dot{M}_{\rm Edd}$, which is reduced by one order of magnitude from those with radiative feedback alone. Furthermore, we find that the critical gas density required for rapid accretion is lower by a factor of ~ 3 nearly independently of BH mass, when mechanical feedback is considered. By studying the dependence on outflow model parameters (e.g., opening angle, mass-loading degree into outflows, velocity), we conclude that contrary to naive expectation, the existence of stronger outflow leads to the transition to rapid accretion phases more efficiently. Rapidly growing BHs inject mechanical power with $\sim 0.1-1\%$ of the radiative luminosity into their host galaxy scales, which is used for cosmological simulations.

Key words: accretion, accretion discs – black hole physics – *(galaxies:)* quasars: supermassive black holes – cosmology: theory

1 INTRODUCTION

Supermassive black holes (SMBHs) with masses of $\gtrsim 10^9\ {\rm M}_\odot$ (e.g. Fan et al. 2004; Mortlock et al. 2011; Wu et al. 2015; Bañados et al. 2018; Matsuoka et al. 2018a,b,c; Onoue et al. 2019) as the central engine of bright quasars at high redshifts $z \gtrsim 6$ (or less than ~ 1 Gyr after the Big Bang) require their rapid growth in the early Universe. Although SMBHs play crucial roles on the history of their host galaxies (e.g. Silk & Rees 1998; King 2003; Murray et al. 2005; Kormendy & Ho 2013, reference theirin), their formation and growth mechanisms are still unclear.

To assemble such monster SMBHs within a certain short timescale, several seeding models have been proposed by many authors (e.g., Volonteri 2012; Haiman 2013; Inayoshi et al. 2019, references therein). One possible candidate of the seed is the stellar-mass BH with $\sim 10-100\ {\rm M}_\odot$ left behind by collapse of the first generation of stars. Assuming that those remnant BHs grow via gas accretion at the corresponding Eddington rate with a 10% of the radiative efficiency, the timescale required to form $\gtrsim 10^9\ {\rm M}_\odot$ SMBHs becomes as long as ~ 1 Gyr, which is comparable to the age of the high-redshift Universe. Therefore, this naive idea could work only if rapid BH accretion with a high duty cycle was sustained over $7-8$ orders of magnitude growth in mass (Tanaka & Haiman 2009).

An alternative candidate is more massive seed BHs with $\sim 10^4-10^6\ {\rm M}_\odot$ formed by direct collapse of supermassive stars or runaway stellar mergers in a dense metal-poor

★ takeo@kusastro.kyoto-u.ac.jp
† inayoshi@pku.edu.cn, corresponding author

© 2020 The Authors

star cluster (Bromm & Loeb 2003; Devecchi & Volonteri 2009; Shang et al. 2010; Regan et al. 2014; Inayoshi et al. 2014; Latif et al. 2016; Tagawa et al. 2019; Chon & Omukai 2020). Such massive seeds are expected to form in high-z protogalaxies under peculiar conditions such as the existence of strong H_2 photodissociating Lyman-Werner radiation (Dijkstra et al. 2008; Johnson et al. 2013; Sugimura et al. 2014; Visbal et al. 2014; Wolcott-Green et al. 2017), high baryon-dark matter streaming velocity, rapid mergers of dark-matter halos, or some combination of these effects (Tanaka & Li 2014; Inayoshi et al. 2018; Wise et al. 2019). Even giving the massive seeds a head start towards SMBHs at $z \gtrsim 6$, the growth timescale would be reduced only by a factor of two under the assumption of Eddington-limited accretion. Therefore, it is worth exploring the possibility that seed BHs embedded in protogalaxies can grow faster breaking the Eddington limit (though the duration should be short enough to be consistent with the Soltan argument) and addressing whether the conditions to trigger super-Eddington accretion are consistent with those of their seeding models.

Rapid gas accretion onto compact objects has been investigated by numerous studies. There are several lines of observational evidence to show both stellar-mass BHs and SMBHs can be super-Eddington accretors; e.g., some ultra-luminous X-ray sources (e.g., King et al. 2001; Watarai et al. 2001) and narrow-line Seyfert-1 galaxies (e.g., Wang et al. 1999; Mineshige et al. 2000). In theory, the properties of super-Eddington accretion have been explored by analytical and numerical work. In the recent decade, radiation (magneto-)hydrodynamical simulations have shown that super-Eddington accreting flows can feed the central BH as long as a sufficient mount of gas already exists or is efficiently supplied to the vicinity of the BH event horizon scale of $\sim 10^{2-3}\ R_{\rm Sch}$ (see also Ohsuga et al. 2009; Ohsuga & Mineshige 2011; Jiang et al. 2014; McKinney et al. 2014; Sądowski et al. 2015; Takahashi et al. 2016; Jiang et al. 2019), where $R_{\rm Sch} \equiv 2GM_{\rm BH}/c^2$ is the Schwarzschild radius, $M_{\rm BH}$ is the BH mass, and c is the speed of light. However, accreting matter at super-Eddington rates release a huge amount of gravitational potential energy as radiation and/or in outflows. Emergent ionizing photons are likely to propagate outward and heat the inflowing gas from the BH gravitational sphere of influence (hereafter, the Bondi radius $R_{\rm B}$). Since gas-pressure gradient force (and partially radiation force exerted through electron scattering) in the ionized region overcomes gravity of the central BH, gas accretion from larger radii to the nuclear BH is strongly suppressed. This quiescent phase lasts until the size of the ionized bubble substantially shrinks because of the combination of radiative recombination and lower radiative luminosity from the BH. As a result, radiative feedback due to photoionization and heating limits the BH feeding rate significantly below the Eddington accretion rate $\dot{M}_{\rm Edd}$ [$\equiv L_{\rm Edd}/(0.1c^2)$] (e.g., Ciotti & Ostriker 2001; Milosavljević et al. 2009a,b; Alvarez et al. 2009; Park & Ricotti 2011, 2012; Jeon et al. 2012), where $L_{\rm Edd}$ is the Eddington luminosity.

However, when the BH is embedded in a dense gas cloud so that the gas inflowing rate from $R_{\rm B}$ exceeds $\sim 500\ \dot{M}_{\rm Edd}$, the inflowing gas structure approaches a steady state without time-dependent oscillations, yielding hyper-Eddington accretion (Inayoshi et al. 2016). The critical accretion rate required to realize hyper-Eddington accretion is rewritten as

$$n_\infty \gtrsim 10^4\ {\rm cm}^{-3} \left(\frac{M_{\rm BH}}{10^5\ {\rm M}_\odot}\right)\left(\frac{T_\infty}{10^4\ {\rm K}}\right)^{3/2}, \quad (1)$$

where n_∞ and T_∞ are density and temperature of the surrounding gas. Note that this inequality is satisfied when the size of an ionized region surrounding an accreting BH, $R_{\rm ion}$ (well approximated by the Strömgren radius) is smaller than the Bondi radius. In this case, since radiation emitted from the BH hardly ionizes and heats the ambient gas, gas inflows that begins to occur from $\sim R_{\rm B}$ are not prevented by radiative feedback, but rather lead to collapse of the ionized region. Several follow-up radiation hydrodynamical (RHD) simulations have shown that when the radiation is emitted preferentially towards the polar regions, rapid gas accretion is allowed through the equatorial region with strong inward ram pressure that leads to collapse of the bipolar ionized region (Takeo et al. 2018; see also Sugimura et al. 2017). We also note that the size of an ionized region depends on spectra of radiation. Takeo et al. (2019) re-evaluated the transition criteria, taking into account more realistic radiation spectra associated with the properties of nuclear accretion discs that depend on the BH mass and accretion rate. They found that the required density is lowered for less massive BHs because the mean photon energy becomes too high to ionize and heat the ambient gas. In addition, when the accreting gas is slightly polluted by heavy elements ($\lesssim 0.01\ Z_\odot$) and contains dust grain, the spectral shape of emergent radiation is softened due to attenuation of ultraviolet photons, making the ionized regions smaller (Yajima et al. 2017; Toyouchi et al. 2019).

The next question is whether mechanical feedback associated with outflows[1] launched from an accretion disc affects the properties of gas inflows from outside $R_{\rm B}$. So far, various mechanisms driving outflows have been proposed. In fact, most numerical simulations of super-Eddington accretion flows show the presence of significant mass outflows driven by radiation pressure (e.g., Ohsuga et al. 2005; Kawashima et al. 2009; Jiang et al. 2014; Sądowski et al. 2015; Jiang et al. 2019). Even with a sub-Eddington accretion rate, strong outflows can be generated owing to the large-scale poloidal magnetic field (e.g., Blandford & Payne 1982; Li & Cao 2019), large line opacity (e.g., Proga et al. 2000; Nomura et al. 2016, 2018), and by extracting the BH spin (Blandford & Znajek 1977). Applying those results to cosmological simulations of galaxy evolution, numerous authors have been investigating the impact of mechanical feedback on BH accretion and star formation in galactic scales at relatively low redshifts (e.g., Dubois et al. 2010; Ostriker et al. 2010; Novak et al. 2011; Choi et al. 2012; Yuan et al. 2018; Qiu et al. 2019).

Recently, Regan et al. (2019) have studied the effect of bipolar jets launched from an accreting seed BH onto gas inflows in an atomic cooling halo, performing cosmological simulations that resolve the BH gravitational influence radius. They found that the jets evacuate the central ~ 0.1 pc around the BH ($\simeq 0.1\ R_{\rm B}$) and limit the accretion rate below

[1] In this paper, "outflow" is defined as mass flow at a non-relativistic velocity. Relativistic (and highly collimated) outflows are phrased as jets.

the Eddington value. In fact, since the jet injection scale is not spatially resolved well, the jets are not sufficiently collimated at the bottom but prevent gas inflows even through the equatorial plane (i.e., perpendicular to the gas angular momentum vector). This leads to overestimate of the mechanical feedback effect. On the other hand, their simulations do not take into account radiative feedback (photoionization and heating), which evacuates gas around the BH and could assist the outflow component in expanding outward and affecting the gas inflow from larger radii. In this sense, the impact of mechanical feedback on gas inflows is underestimated in their simulations (see discussion in §3.3).

In this paper, we explore the conditions required for hyper-Eddington accretion onto a BH when both radiative and mechanical feedback operate simultaneously, performing two-dimensional hydrodynamical simulations with multi-frequency radiation transfer. We conduct a comprehensive survey on the parameter dependence of outflow models, varying the outflow opening angle, mass-loading degree into outflows, velocity of outflows, and density of gas surrounding the BH. To model mechanical feedback, we adopt a phenomenological model proposed by Ostriker et al. (2010), while radiative feedback is treated by adopting the standard and slim disc model (Shakura & Sunyaev 1973; Abramowicz et al. 1988; Watarai 2006) as in Takeo et al. (2019). We find that the flow structure consists of two distinct parts in the early sub-Eddington phase; the bipolar outflowing region heated up to $T \sim 10^{6-7}$ K due to strong shock and the equatorial inflowing region where ionized gas is mildly heated to $T \sim 10^5$ K due to photoionization. When the ambient gas density exceeds a critical threshold, as in the cases where only radiative feedback is included (Inayoshi et al. 2016; Takeo et al. 2018), the mass accretion rate onto the nuclear region rises to a hyper-Eddington value. Since mechanical power of outflows driven by the rapidly accreting BH is sufficiently strong, bipolar outflows completely evacuate the surrounding gas in the polar region and reduce the mass inflow (BH accretion) rate by a factor of $\approx 3-13$ ($\approx 6-26$, respectively) from the case without mechanical feedback. Furthermore, we find that the critical gas density required for hyper-Eddington accretion is reduced by a factor of ~ 3 and the transition occurs in a shorter dynamical timescale when mechanical feedback is modelled in the simulations. In fact, the effects that alleviate the transition to rapid accretion tend to be more prominent as the outflow is stronger, i.e., a wider opening angle, higher mass-loading factor, and higher outflow velocity. This is because suppression of BH accretion owing to outflows reduces the radiative output from the nuclear BH, leading to hyper-Eddington accretion.

The rest of this paper is organized as follows. In §2, we describe our numerical setup and list the models we study. In §3, we present the simulation results and discuss their dependence on the outflow properties. In §4, we derive the conditions required for the transition to hyper-Eddington accretion and briefly discuss Impact of BH feedback on the host galaxy evolution. Finally, we summarize our findings in §5.

2 METHODS

In this paper, we study the properties of rapid gas inflows onto a BH supplied from larger scales ($\gg R_{\rm Sch}$), performing axisymmetric two-dimensional radiation hydrodynamical simulations. To investigate the effects of radiative and mechanical feedback on the gas dynamics, our simulations resolve the BH gravitational sphere of influence, the so-called Bondi radius (Bondi 1952), defined by

$$R_{\rm B} \equiv \frac{GM_{\rm BH}}{c_\infty^2} \simeq 1.97\times10^{19}\ {\rm cm}\ \left(\frac{M_{\rm BH}}{10^5\ {\rm M}_\odot}\right)\left(\frac{T_\infty}{10^4\ {\rm K}}\right)^{-1}, \quad (2)$$

where $c_\infty \equiv \sqrt{\gamma \mathcal{R} T_\infty/\bar{\mu}}$ is the sound speed, γ is the specific heat ratio, $\mathcal{R}$ is the gas constant, and $\bar{\mu}$ is the mean molecular weight. Within the Bondi radius, the BH gravitational energy dominates over the thermal energy of the gas, and thus gas accretion begins to occur unless feedback associated with BH feeding plays an important role. We also define the Bondi accretion rate for isothermal gas as

$$\dot{M}_{\rm B} \equiv \pi e^{3/2}\rho_\infty \frac{G^2M_{\rm BH}^2}{c_\infty^3}, \quad (3)$$

$$\simeq 7\times10^3\ \dot{M}_{\rm Edd}\left(\frac{M_{\rm BH}}{10^5\ {\rm M}_\odot}\right)\left(\frac{n_\infty}{10^5\ {\rm cm}^{-3}}\right)\left(\frac{T_\infty}{10^4\ {\rm K}}\right)^{-3/2}. \quad (4)$$

Throughout this paper, the Bondi radius and rate are calculated by setting $\gamma = 1$, $\bar{\mu} = 1.23$ and $T_\infty = 10^4$K as reference values, although those values are simulated self-consistently.

2.1 Basic equations

We solve the axisymmetric two-dimensional hydrodynamical equations using a code developed in Takahashi & Ohsuga (2013) which compute the flux with the Harten-Lax-vanLeer Riemann solver (Harten et al. 1983) and ensures the second order accuracy in space and time (van Leer 1977). Here we employ spherical coordinates of $(r,\ \theta,\ \phi)$ with the polar axis ($\theta = 0$ and π) perpendicular to the equatorial plane ($\theta = \pi/2$).

The hydrodynamical equations are the following: the equation of continuity

$$\frac{\partial\rho}{\partial t} + \nabla\cdot(\rho\boldsymbol{v}) = \dot{\rho}_{\rm out}, \quad (5)$$

the equations of motion

$$\frac{\partial(\rho v_r)}{\partial t} + \nabla\cdot(\rho v_r\boldsymbol{v}) = -\frac{\partial p}{\partial r} + \rho\left(\frac{v_\theta^2}{r} + \frac{v_\phi^2}{r}\right) - \rho\frac{\partial\psi}{\partial r} + f_{\rm rad} + \dot{p}_{\rm out}, \quad (6)$$

$$\frac{\partial(\rho r v_\theta)}{\partial t} + \nabla\cdot(\rho r v_\theta\boldsymbol{v}) = -\frac{\partial p}{\partial\theta} + \rho v_\phi^2\cot\theta, \quad (7)$$

$$\frac{\partial(\rho r v_\phi\sin\theta)}{\partial t} + \nabla\cdot(\rho r v_\phi\sin\theta\boldsymbol{v}) = 0, \quad (8)$$

and the energy equation

$$\frac{\partial e}{\partial t} + \nabla\cdot[(e+p)\boldsymbol{v}] = -\frac{GM_{\rm BH}\rho}{r^2}v_r - \Lambda + \Gamma + \dot{e}_{\rm out}. \quad (9)$$

where ρ is the gas density, $\boldsymbol{v} = (v_r, v_\theta, v_\phi)$ is the velocity vector, p is the gas pressure, and $f_{\rm rad}$ is the outward radiation force onto the radial direction. We take into account gravitational force of the central BH ($r = 0$) and neglect the gas

self-gravity. Since the general relativistic effect is negligible around $R_{\rm B}(\gg R_{\rm Sch})$, the gravitational potential is given by $\psi = -GM_{\rm BH}/r$. The total energy per volume (in erg cm^{-3}) is defined by $e \equiv e_{\rm int} + \rho|\boldsymbol{v}|^2/2$, $e_{\rm int}$ is the gas internal energy density, Λ is the radiative cooling rate, and Γ is the radiative heating rate. We assume the equation of state of ideal gas as $p = (\gamma - 1)e_{\rm int}$ for $\gamma = 5/3$. To ensure the mass, momentum and energy conservation, we add source terms associated with mechanical feedback ($\dot{\rho}_{\rm out}$, $\dot{p}_{\rm out}$, and $\dot{e}_{\rm out}$).

We consider cooling processes associated with H, He, He$^+$ atoms and free-free emission (Glover & Jappsen 2007), adopting the optically-thin cooling rates. We solve chemical reaction networks including six species of H, H$^+$, He, He$^+$, He^{++}, and e$^-$. The abundance of He nuclei relative to H nuclei is set to 8.33×10^{-2}. Here we adopt the chemical processes of photoionization, collisional ionization and radiative recombination (Abel et al. 1997; Glover & Jappsen 2007), including the secondary ionization (see Section 2.3). Since photoionization due to diffusive recombination photons is negligible, we adopt the on-the-spot approximation where the case A recombination rate is replaced by the case B rate. In order to solve the basic equations stably, the source terms associated with radiative cooling/heating in the energy equation and the chemical reaction networks are updated with a fully implicit method. Throughout our simulations, we set the time step to the Courant timescale (the Courant number is set to 0.4).

2.2 Mechanical feedback

To study the impact of mechanical feedback due to outflows on gas inflow, we adopt a phenomenological model proposed by (Ostriker et al. 2010), where conservation of mass, momentum and energy is taken into account. Defining the mass inflow through the innermost radius of $r_{\rm min}$ (see Section 2.5) as

$$\dot{M}_{\rm in} = \int_{v_r<0} {\rm d}\Omega\, r_{\rm min}^2\, \rho|v_r|, \tag{10}$$

and the mass loading factor into outflows as $\beta_{\rm out} \equiv \dot{M}_{\rm out}/\dot{M}_{\rm BH}$, we obtain the mass outflow rate and BH accretion rate from mass conservation,

$$\dot{M}_{\rm out} = \frac{\beta_{\rm out}}{1+\beta_{\rm out}}\dot{M}_{\rm in}, \tag{11}$$

$$\dot{M}_{\rm BH} = \frac{1}{1+\beta_{\rm out}}\dot{M}_{\rm in}. \tag{12}$$

Here, it is worthy noting the following two things that are natural consequences from mass conservation but sometimes misinterpreted. Note that mass conservation ensures that the outflow mass rate never exceeds the inflow rate even in the limit of $\beta_{\rm out} \gg 1$. In the same limit, the BH accretion rate goes to zero no matter how much mass inflow rate exists at $r = r_{\rm min}$.

Next, we define the total momentum and energy input due to outflows as

$$\dot{P}_{\rm out} = \dot{M}_{\rm out} v_{\rm out}, \tag{13}$$

$$\dot{E}_{\rm out} = \frac{1}{2}\dot{M}_{\rm out} v_{\rm out}^2, \tag{14}$$

where $v_{\rm out}$ is the outflow velocity injected at $r = r_{\rm min}$. Throughout this paper, we treat $\beta_{\rm out}$ and $v_{\rm out}$ as free parameters varying those values and discuss the dependence on the result (see §3.3). The mass, momentum, and energy of outflows are injected at the inner-most grid as source terms $\dot{\rho}_{\rm out}$, $\dot{p}_{\rm out}$ and $\dot{e}_{\rm out}$ in an anisotropic way:

$$\dot{\rho}_{\rm out} = \frac{\dot{M}_{\rm out}}{4\pi r_{\rm min}^2 C}\mathcal{G}(\theta)\delta(r - r_{\rm min}), \tag{15}$$

$$\dot{p}_{\rm out} = \frac{\dot{P}_{\rm out}}{4\pi r_{\rm min}^2 C}\mathcal{G}(\theta)\delta(r - r_{\rm min}), \tag{16}$$

$$\dot{e}_{\rm out} = \frac{\dot{E}_{\rm out}}{4\pi r_{\rm min}^2 C}\mathcal{G}(\theta)\delta(r - r_{\rm min}). \tag{17}$$

Here, $\mathcal{G}(\theta)$ characterizes the angular dependence of outflows as

$$\mathcal{G}(\theta) = \begin{cases} 1 & , \ 0^\circ \le \theta \le \widetilde{\theta}_{\rm out} \\ \exp\left(-\left(\dfrac{\theta - \widetilde{\theta}_{\rm out}}{\Delta\theta}\right)^2\right) & , \ \widetilde{\theta}_{\rm out} \le \theta \le 90^\circ, \end{cases} \tag{18}$$

where $C \equiv \int_0^{\pi/2} {\rm d}\theta \sin\theta\ \mathcal{G}(\theta)$, δ is the Dirac delta-function, $\widetilde{\theta}_{\rm out} = \theta_{\rm out} - 2\Delta\theta$, and we set $\Delta\theta = 6^\circ$ (see also Sugimura et al. 2017; Ciotti et al. 2017).

2.3 Radiation transfer and radiative feedback

To estimate the radiative heating rate Γ, ionization rate $k_{\rm ph}$, and radiation force $f_{\rm rad}$, we need to solve for radiation quantities in the accreting gas. In this paper, we adopt the same treatment of radiation transfer as described in our previous work (Inayoshi et al. 2016; Takeo et al. 2018, 2019).

The multi-frequency radiative transfer equation is give by

$$\frac{1}{r^2}\frac{\rm d}{{\rm d}r}(r^2 F_\nu) = -\rho\kappa_\nu c E_\nu, \tag{19}$$

where F_ν is the radiation flux, E_ν is the radiation energy density, and κ_ν is the absorption opacity. Here, the radiation field is assumed to be steady because the light crossing time is much shorter than the hydrodynamical time step. We take into account only the radial component of radiation flux because non-radial components are negligible (see §4 in Takeo et al. 2018 for more details). The frequency range is set to $h\nu_{\rm min}(= 13.6\ {\rm eV}) \le h\nu \le h\nu_{\rm max}(= 100\ {\rm keV})$, where h is the Planck constant. Inside the ionized region, the gas is optically thin even to ionizing photons and thus $E_\nu \simeq F_\nu/c$. Therefore, the radiation transfer equation is approximated in a simple form:

$$\frac{1}{r^2}\frac{\rm d}{{\rm d}r}(r^2 F_\nu) = -\rho\kappa_\nu F_\nu. \tag{20}$$

The ionization coefficients and photoionization heating rates are calculated by using the photon-conserving method (Whalen & Norman 2006). The primary ionization rates $k_{{\rm ph},i}^{\rm p}$ (i = H, He, and He$^+$) are given by

$$k_{{\rm ph},i}^{\rm p} = \int_{\nu_{\rm min}}^{\nu_{\rm max}} {\rm d}\nu\ \frac{F_\nu}{h\nu}\ \sigma_{{\rm bf},i}, \tag{21}$$

where $\sigma_{{\rm bf},i}$ is the bound-free cross section. Energetic electrons produced by primary ionization can further contribute

Table 1. Simulation Runs and Input Parameters. Column (1) model ID, (2) BH mass, (3) ambient gas density, (4) outflow opening angle, (5) mass loading factor, (6) outflow velocity, and (7) the transition epoch in units of the dynamical time at the Bondi radius; $t_{\rm dyn} = 8.4 \times 10^5\ (M_{\rm BH}/10^5\ {\rm M}_\odot)$ yr. For all the models, isotropic radiation is assumed in the early stage before the transition to rapid accretion occurs. For the first three models (A45M5-), we extend the simulations to the late stage after the transition epoch, varying the feedback model parameters: anisotropic radiation with an opening angle of $\theta_{\rm rad} = 45°$ (A45M5), anisotropic radiation with $\theta_{\rm rad} = 45°$ and $\beta_{\rm out} = 10$ (A45M5-B10), and isotropic radiation but assuming a diluted blackbody spectrum (A45M5-B1-iso). In Model RAD, only radiative feedback is considered as reference.

Model	$M_{\rm BH}$ ($M_\odot$)	n_∞ (cm^{-3})	$\theta_{\rm out}$ (°)	$\beta_{\rm out}$	$v_{\rm out}$ (km s^{-1})	$t_{\rm tran}$ ($t_{\rm dyn}$)	Reference
A45M5 (fiducial)	10^5	1×10^5	45	1	1000	0.96	§3.1
A45M5-B10	10^5	1×10^5	45	10	1000	–	§3.2.1
A45M5-B1-iso	10^5	1×10^5	45	1	1000	–	§3.2.2
A60M5	10^5	1×10^5	60	1	1000	0.84	§3.3
A80M5	10^5	1×10^5	80	1	1000	0.62	§3.3
V500M5	10^5	1×10^5	80	1	500	0.71	§3.3
V333M5	10^5	1×10^5	80	1	333	0.75	§3.3
V200M5	10^5	1×10^5	80	1	200	0.88	§3.3
B01M5	10^5	1×10^5	80	0.1	1000	0.79	§3.3
B001M5	10^5	1×10^5	80	0.01	1000	1.3	§3.3
T34M5	10^5	3×10^4	80	1	1000	1.7	§4.1
T24M5	10^5	2×10^4	80	1	1000	2.5	§4.1
T14M5	10^5	1×10^4	80	1	1000	–	§4.1
T33M5	10^5	3×10^3	80	1	1000	–	§4.1
T18M1	10	1×10^8	80	1	1000	0.79	§4.1
T57M1	10	5×10^7	80	1	1000	1.3	§4.1
T37M1	10	3×10^7	80	1	1000	1.8	§4.1
T17M1	10	1×10^7	80	1	1000	–	§4.1
RAD (w/o outflows)	10^5	1×10^5	–	–	–	1.3	

to ionization of nearby atoms (secondary ionization, e.g., Shull & van Steenberg 1985). The secondary ionization rates for species j = H, and He are

$$k^{\rm s}_{{\rm ph},j} = \sum_{i={\rm H,He}} \int_{\nu_{\rm min}}^{\nu_{\rm max}} {\rm d}\nu\ \frac{F_\nu}{h\nu}\ \sigma_{{\rm bf},j}\ \Phi^j(E_i, x_{\rm H^+})\ \frac{x_i}{x_j}, \tag{22}$$

where x_j is the abundance of species j, $\Phi^j(E_i, x_{\rm H^+})$ is the fraction of secondary ionization of species j per primary electron of energy $E_i \equiv h\nu - I_i$, and I_i is the ground state ionization potential of the species i. Thus, the photoionization rate is given by the sum of primary and secondary ionization rate.

The photoionization heating rate (i = H, He, and He$^+$) is calculated as

$$\Gamma_i = \int_{\nu_{\rm min}}^{\nu_{\rm max}} {\rm d}\nu\ \frac{F_\nu}{h\nu}\ \sigma_{{\rm bf},i}\ E_h(E_i, x_{\rm H^+}), \tag{23}$$

E_h is the energy of a primary electron deposited as heat. We adopt the functional forms of $\Phi^{\rm H}$, $\Phi^{\rm He}$, and E_h (Ricotti et al. 2002). Note that secondary ionization of He$^+$ is negligible (Shull & van Steenberg 1985).

The radiation force caused by electron scattering and bound-free transition is calculated by

$$f_{\rm rad} = \frac{n x_{\rm e}}{c} \int_{\nu_{\rm min}}^{\nu_{\rm max}} \sigma_{\rm es} F_\nu {\rm d}\nu + \frac{\Gamma^{\rm p}}{c}, \tag{24}$$

where $\Gamma^{\rm p}$ is the sum of the heating rates owing to primary ionization of H, He, and He$^+$.

2.4 Radiation spectra and anisotropy

To quantify the effect of radiative feedback (photoionization and heating), we take into account radiation spectra that depend on BH mass and accretion rate at each time step. Following Takeo et al. (2019), we adopt a multicolour blackbody spectrum (e.g., Kato et al. 2008), since the accretion rate onto the BH is always high enough ($\dot{M}_{\rm BH}/\dot{M}_{\rm Edd} \gtrsim 10^{-2}$) for the nuclear disc to be optically thick. The specific radiation luminosity is give by

$$L_\nu = 2 \int_{R_{\rm in}}^{R_{\rm out}} {\rm d}R\ 2\pi R\ B_\nu[T_{\rm eff}(R)], \tag{25}$$

where $B_\nu(T_{\rm eff})$ is the blackbody intensity with an effective temperature of $T_{\rm eff}$, $R_{\rm in} (\simeq 1.1 - 1.7\ R_{\rm Sch})$ and $R_{\rm out} (= 10^4\ R_{\rm Sch})$ are the locations of the disc inner and outer edge, respectively (see more details in Takeo et al. 2019). For both sub-Eddington and super-Eddington regimes, the radial profile of the effective temperature is given by

$$T_{\rm eff}(R) = 2.5 \times 10^6\ {\rm K} \left(\frac{M_{\rm BH}}{10^5\ {\rm M}_\odot}\right)^{-1/4} \left(\frac{R}{R_{\rm Sch}}\right)^{-1/2} f^{1/8} \mathcal{F}, \tag{26}$$

where f and $\mathcal{F}$ are functions that connects the standard and slim disc solution smoothly (see the details in Watarai 2006). Note that for a accretion rate of $\dot{m}_{\rm BH} (\equiv \dot{M}_{\rm BH}/\dot{M}_{\rm Edd}) \gg 1$, $f \simeq 1$ and $\mathcal{F} \simeq 1$ inside the photon-trapping radius of $R_{\rm tr} \equiv \dot{m}_{\rm BH} R_{\rm Sch}$, within which the advection timescale is shorter than the photon diffusion timescale. Using this equation, the bolometric luminosity of radiation from a slim disc is

expressed as

$$\frac{L}{L_{\rm Edd}} = 2\left[1 + \ln\left(\frac{\dot{m}_{\rm BH}}{2}\right)\right], \quad (27)$$

for $\dot{m}_{\rm BH} > 2$, otherwise $L/L_{\rm Edd} = \dot{m}_{\rm BH}$ (Watarai et al. 2000).

We assume radiation field to be isotropic, i.e., $F_\nu(r = r_{\rm min}) = L_\nu/(4\pi r_{\rm min}^2)$ when the BH accretion rate is as low as $\dot{m}_{\rm BH} \leq 4$ (although the radiative flux from a geometrically thin disc has an angular dependence of $F_\nu \propto |\cos\theta|$). This treatment gives us conservative conditions required for the transition to rapid accretion phases because highly anisotropic radiation does not prevents gas inflows from the equatorial region which cover a large solid angle. After the transition of gas inflow into hyper-Eddington accretion, the nuclear disc is likely to be geometrically thick with $H/R \simeq 0.3-0.5$ (Abramowicz et al. 1988), and thus radiation is emitted preferentially towards the poles (Ohsuga et al. 2005; Jiang et al. 2014; Sądowski et al. 2015). Therefore, we assume anisotropic radiation with an opening angle of $\theta_{\rm rad} = 45°$ as a fiducial case after the transition (same as outflows). In addition, we study a case with isotropic radiation even after the transition in §3.2.2 to conservatively discuss the stability of a hyper-Eddington phase because isotropic radiation can prevent the gas inflow from the equatorial region (see also Takeo et al. 2018).

2.5 initial and boundary conditions

To solve the basic equations, we employ spherical coordinates with a logarithmically spaced grid in the radial direction ($r_{\rm min} \leq r \leq r_{\rm max}$) and a uniformly-spaced grid in the polar direction ($0 \leq \theta \leq \pi$; $\theta = \pi/2$ corresponds to the equator). Since we study the gas dynamics over a wide range of spatial scales that cover the Bondi radius and includes its interior, we adopt $(r_{\rm min},\ r_{\rm max}) = (0.007\ R_{\rm B},\ 6\ R_{\rm B})$. The numbers of the grid cells are set to $(N_r,\ N_\theta) = (60, 120)$. We note that the number of the radial grids in this study is lower than that in our previous work, where $N_r = 100$ is set (Takeo et al. 2018), in order to reduce the computational time but stably calculate mass flow with a high Mach number $\gg 1$ near the polar regions.

As our initial conditions, we set a neutral uniform and static ($\boldsymbol{v} = 0$) gas cloud with a density n_∞ and temperature $T_\infty = 10^4$ K surrounding a BH with a mass of $M_{\rm BH}$. The BH mass is assumed to be constant throughout the simulations. We impose the absorption inner boundary conditions for the gas density, gas pressure, and velocity to be damped smoothly (e.g. Kato et al. 2004), and the free outer-boundary conditions for three components of the velocity. The reflection symmetry with respect to the polar axis is imposed for non-radial components of the velocity.

To study the impact of mechanical feedback on BH accretion, we explore a wide range of the parameters to characterize outflow power: the outflow opening angle $45° \leq \theta_{\rm out} \leq 80°$, the mass loading factor $0.01 \leq \beta_{\rm out} \leq 10$, and the outflow velocity 100 km s^{-1} $\leq v_{\rm out} \leq$ 1,000 km s^{-1}. In Table 1, we summarize the models we study in this work.

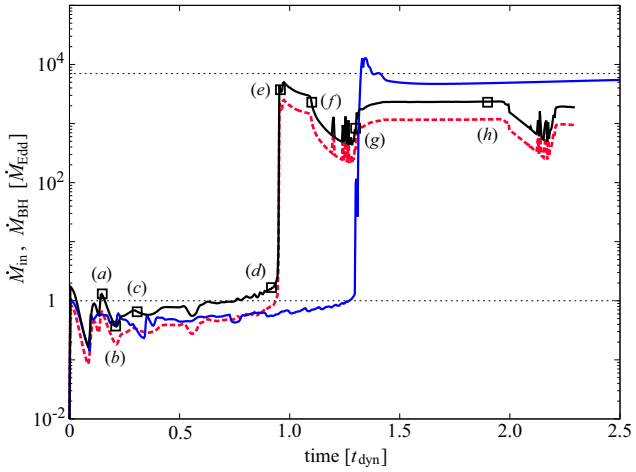


Figure 1. Time evolution of mass inflow rates $\dot{M}_{\rm in}$ (in units of $\dot{M}_{\rm Edd}$) through $r = r_{\rm min}$ for a BH mass of $M_{\rm BH} = 10^5$ M$_\odot$ ($n_\infty = 10^5$ cm^{-3} and $T_\infty = 10^4$ K are assumed as initial conditions) with both radiative and mechanical feedback (black, Model A45M5) and with radiative feedback alone (blue; Model RAD). With mechanical feedback, the model parameters of outflow are set to $\theta_{\rm out} = 45°$, $\beta_{\rm out} = 1$ and $v_{\rm out} = 1,000$ km s^{-1}, and the BH accretion rate is shown by red dashed curve. For both the cases, the BH accretion rate is limited below the Eddington value (lower dotted line) and has a big jump at $t \simeq t_{\rm dyn}$ to a rate as high as the Bondi accretion rate (upper dotted line). Open squares mark the eight epochs (phases *a*-*h*) at which the 1D radial profiles and 2D contours are shown in Figs. 2, 3, 4 and 5. While mechanical feedback makes the transition to rapid accretion occur earlier, the mass inflow and BH accretion rate after the transition are reduced from the case with radiation alone by a factor of $\simeq 3$ and 6, respectively.

3 RESULTS

3.1 Super-Eddington accretion flows exposed to radiative and mechanical feedback

First, we discuss our fiducial case of a massive seed BH with $M_{\rm BH} = 10^5$ M$_\odot$ surrounded by gas with density of $n_\infty = 10^5$ cm^{-3}. The corresponding Bondi and Eddington accretion rates are $\dot{M}_{\rm B} = 15$ M$_\odot$ yr^{-1} and $\dot{M}_{\rm Edd} = 2.1 \times 10^{-3}$ M$_\odot$ yr^{-1} (i.e., $\dot{M}_{\rm B}/\dot{M}_{\rm Edd} = 7 \times 10^3$). The model parameters for outflow injected at $r = r_{\rm min}$ are set to $\theta_{\rm out} = 45°$, $\beta_{\rm out} = 1$ (i.e., $\dot{M}_{\rm BH} = \dot{M}_{\rm out} = 0.5\ \dot{M}_{\rm in}$), and $v_{\rm out} = 1,000$ km s^{-1}. Radiation field is assumed to be isotropic when the accretion rate is a nearly or sub-Eddington value. As seen below, the accretion flow turns into a hyper-Eddington phase, where radiation produced from the geometrically-thick accretion disc is supposed to be anisotropic. In that case, therefore we consider anisotropic radiation field collimated with an opening angle of $\theta_{\rm rad} = 45°$ from the pole (see §3.1.2).

Fig. 1 shows the time evolution of mass inflow rate $\dot{M}_{\rm in}$ through $r = r_{\rm min}$ and BH accretion rate $\dot{M}_{\rm BH}$ with both radiative and mechanical feedback (black and red curves, respectively; Model A45M5). For reference, we also present the case with radiative feedback alone (blue curve; Model RAD) where isotropic radiation is assumed throughout the simulation. With radiation feedback alone, mass accretion occurs episodically and the time-averaged rate is limited to $\lesssim \dot{M}_{\rm Edd}$. The mass inflow rate becomes less time-dependent as time goes and abruptly rises to a rate as high as $\sim \dot{M}_{\rm B}$

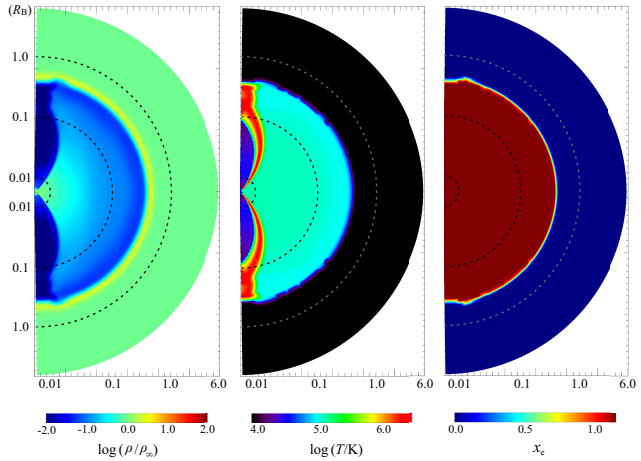


Figure 2. Two-dimensional distribution of the gas density (left), temperature (middle), and ionization degree (right) for Model A45M5 in the phase (*a*) shown in Fig. 1. The flow structure is divided into the bipolar outflowing polar region and the equatorial inflowing region, both of which are embedded in an almost spherical ionized region.

at $t \simeq 1.3\ t_{\rm dyn}$. After the transition, the mass inflow rate becomes constant and thus the accretion flow settles down to a steady state, where ram pressure of the inflow overcomes momentum of incident radiation with luminosity of $L/L_{\rm Edd} \simeq 20$. This transition behaviour has also been found in previous studies with different simulation codes (see Inayoshi et al. 2016; Takeo et al. 2018; Toyouchi et al. 2019 for more details).

In the case with both radiative and mechanical feedback, the overall behaviour of mass inflow rate is qualitatively similar, but there are remarkable differences from the case without outflows. In fact, the mass inflow rate before the transition is twice higher (though the BH accretion rate is comparable) than those in the case with radiation alone, and the transition of accretion flows to a hyper-Eddington phase occurs earlier. This suggests that contrary to naive expectation, mechanical feedback *does* promote the transition (see discussion in §4.1). After the transition when powerful outflows inject mechanical momentum of $\gtrsim 30\ L_{\rm Edd}/c$ into the polar region, the mass inflow and BH accretion rate are reduced by a factor of $\simeq 3$ and 6, respectively. However, the reduced accretion rate is still as high as $\sim 10^3\ \dot{M}_{\rm Edd}$.

In what follows, we show the detailed structure of accretion flows in our fiducial case (Model A45M5) and describe how mechanical feedback affects the accretion flow from the Bondi scale in more details, dividing the entire episode into two epochs before and after the transition.

3.1.1 Episodic accretion owing to radiative feedback

In Fig. 2, we show the two-dimensional distribution of gas density (left), temperature (middle) and ionization degree (right) at $t/t_{\rm dyn} = 0.15$ (phase *a* in Fig. 1). Fig. 3 presents the radial profiles of gas density (top), temperature (middle), radial velocity (bottom) along the pole (solid) and equator (dashed) at three different epochs in the early stage; $t/t_{\rm dyn} = 0.15$ (black; phase *a*), 0.21 (blue; phase *b*), and 0.31 (red; phase *c*). In the bottom panel, we show only the outflow component along the pole and inflow component along the equator.

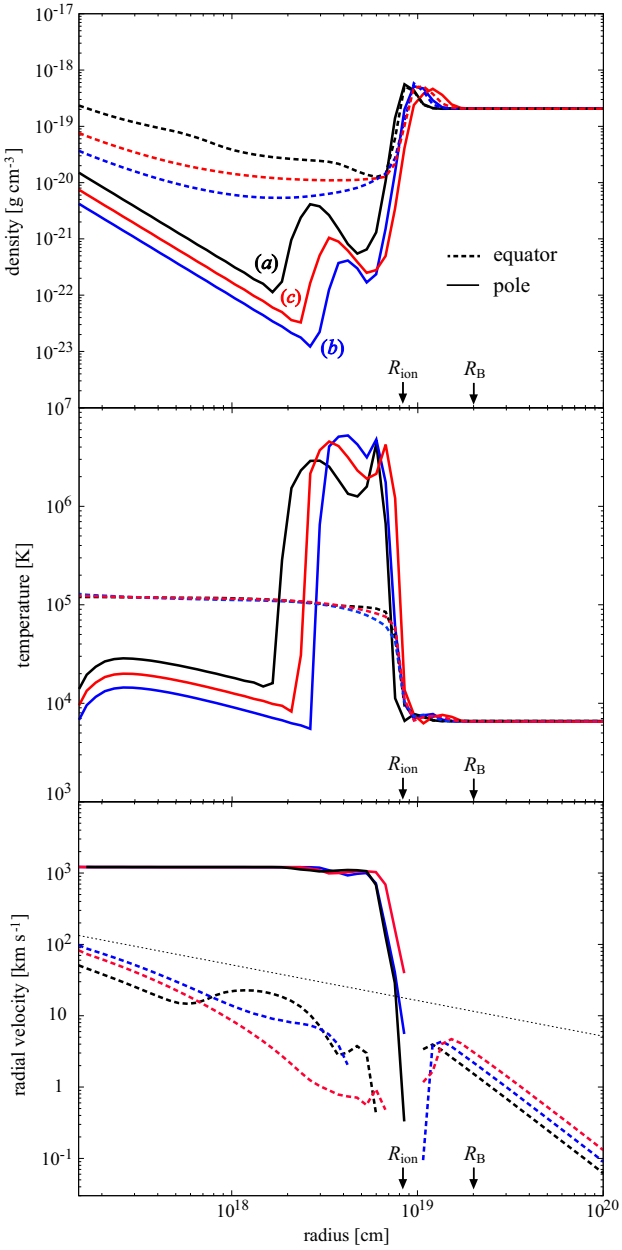


Figure 3. Radial structure of the gas density (top), temperature (middle), radial velocity (bottom) for Model A45M5 at three different epochs: $t/t_{\rm dyn} = 0.15$ (phase *a*; black), 0.21 (phase *b*; blue), and 0.31 (phase *c*; red). The solid and dashed curves present the profiles along the pole ($\theta = 0°$) and equator ($\theta = 90°$). In the bottom panels, only the outflow component along the pole and inflow component along the equator are shown. The dotted line shows the free-fall velocity. In the early stage, radiative and mechanical feedback heats and evacuates gas within the ionized region ($R_{\rm ion}$), but do not affect the dynamics around the Bondi radius for neutral gas ($R_{\rm B}$) substantially.

In the early stage, ionizing radiation emitted from the central accreting BH heats the surrounding gas and forms a nearly spherical low-density cavity until the ionization front reaches $\simeq 0.5\ R_{\rm B}$. In the ionized region with $T \simeq 10^5$ K, the outflow associated with mechanical feedback blows the

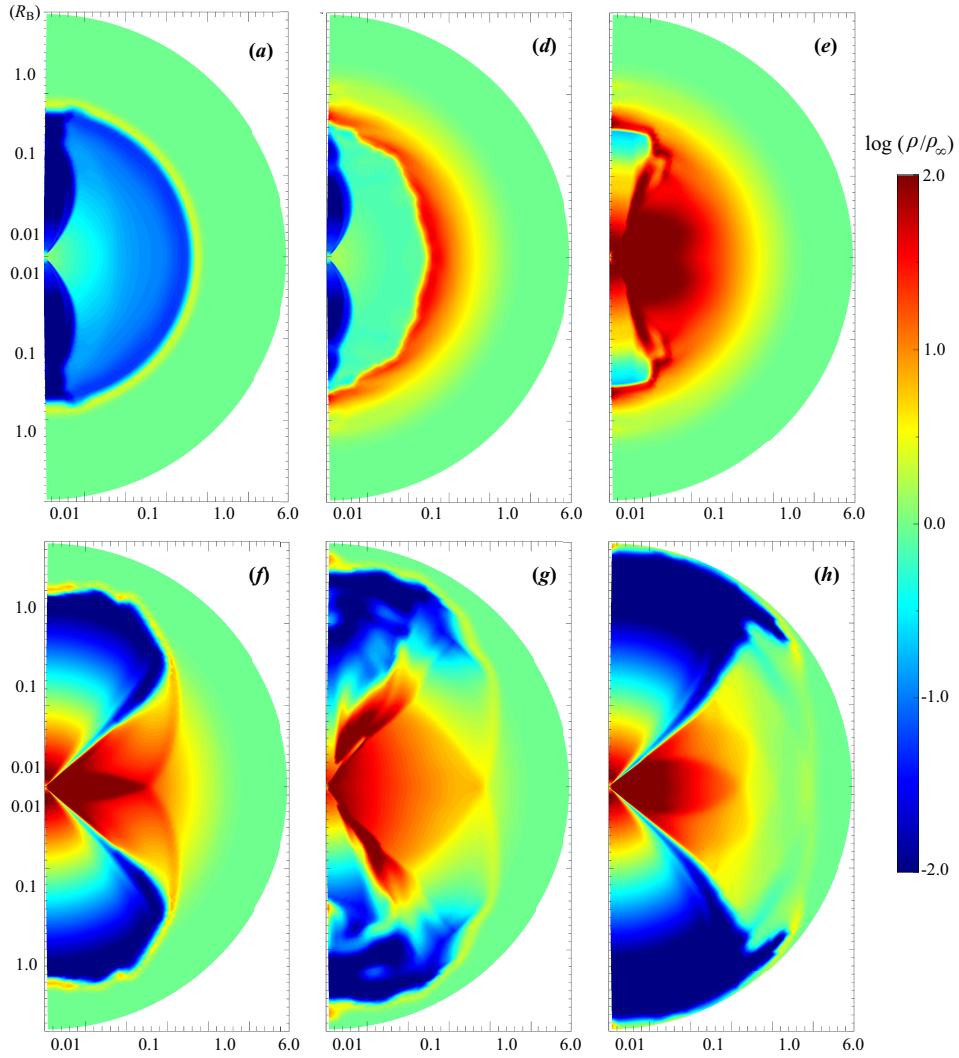


Figure 4. Two-dimensional distribution of the gas density for Model A45M5 at different elapsed times: (*a*) $t/t_{\rm dyn}$ = 0.15, (*d*) 0.92, (*e*) 0.96, (*f*) 1.1, (*g*) 1.3, and (*h*) 1.9. In the early stage (phases *a* and *d*), the ionized region is confined within the Bondi radius and both radiative and mechanical feedback do not affect the gas properties at larger radii. In the transition epoch (phases *e* and *f*), the ionized region begins to collapse due to intense inflow of neutral gas through the equatorial region and then the mass inflow at rates of $\dot{m}_{\rm in} \gtrsim 2 \times 10^3$ produces powerful bipolar outflows. In the late stage (phases *g* and *h*), the bipolar outflows and emergent anisotropic radiation evacuate gas in the polar region completely, but a high inflow rate of $\langle \dot{m}_{\rm in} \rangle \sim 10^3$ is sustained.

gas outward and creates even lower-density cavities near the poles where gas cools owing to adiabatic expansion. The outflow collides with the surrounding gas and forms shocked gas with temperature of $\sim 10^{6-7}$ K, which corresponds to the post-shock temperature of the pre-shock outflowing matter at a velocity of 1,000 km s^{-1}. Although the outflow velocity is ten times higher than the escape velocity from the innermost grid, the mechanical power ($\dot{P}_{\rm out} \simeq 0.015\, L_{\rm Edd}/c$) is not strong enough to break the surrounding medium.

In the equatorial region, where the mechanical momentum of outflows is not injected, the gas begins to accrete from the sonic point for the ionized gas, $R_{\rm B,ion} \equiv GM_{\rm BH}/c_{\rm ion}^2 \sim 2 \times 10^{18}$ cm, where $c_{\rm ion}$ is the sound speed of the ionized gas. On the contrary, gas outside $R_{\rm B,ion}$ is pushed outward by the negative pressure gradient force. As the ionized gas is depleted in the cavity and the outward gas pressure force decreases, a density bump forms just inside the edge of the ionized region near the equator. Finally, the density bump exerted by the inward gas pressure (i.e. $dp/dr > 0$) falls into the central BH (phase *c*). However, radiative and mechanical feedback regulates further mass accretion, leading to episodic accretion several times before the transition occurs. We note that this oscillatory behaviour is caused by the same mechanism as studied in previous work (e.g. Ciotti & Ostriker 2001; Milosavljević et al. 2009a; Park & Ricotti 2011, 2012; Inayoshi et al. 2016).

3.1.2 *Transition to hyper-Eddington accretion with powerful bipolar outflows*

In Figs. 4 and 5, we present the two-dimensional density distribution and the radial profiles of physical quantities at the early stage (phase *a*) and several different epochs in the

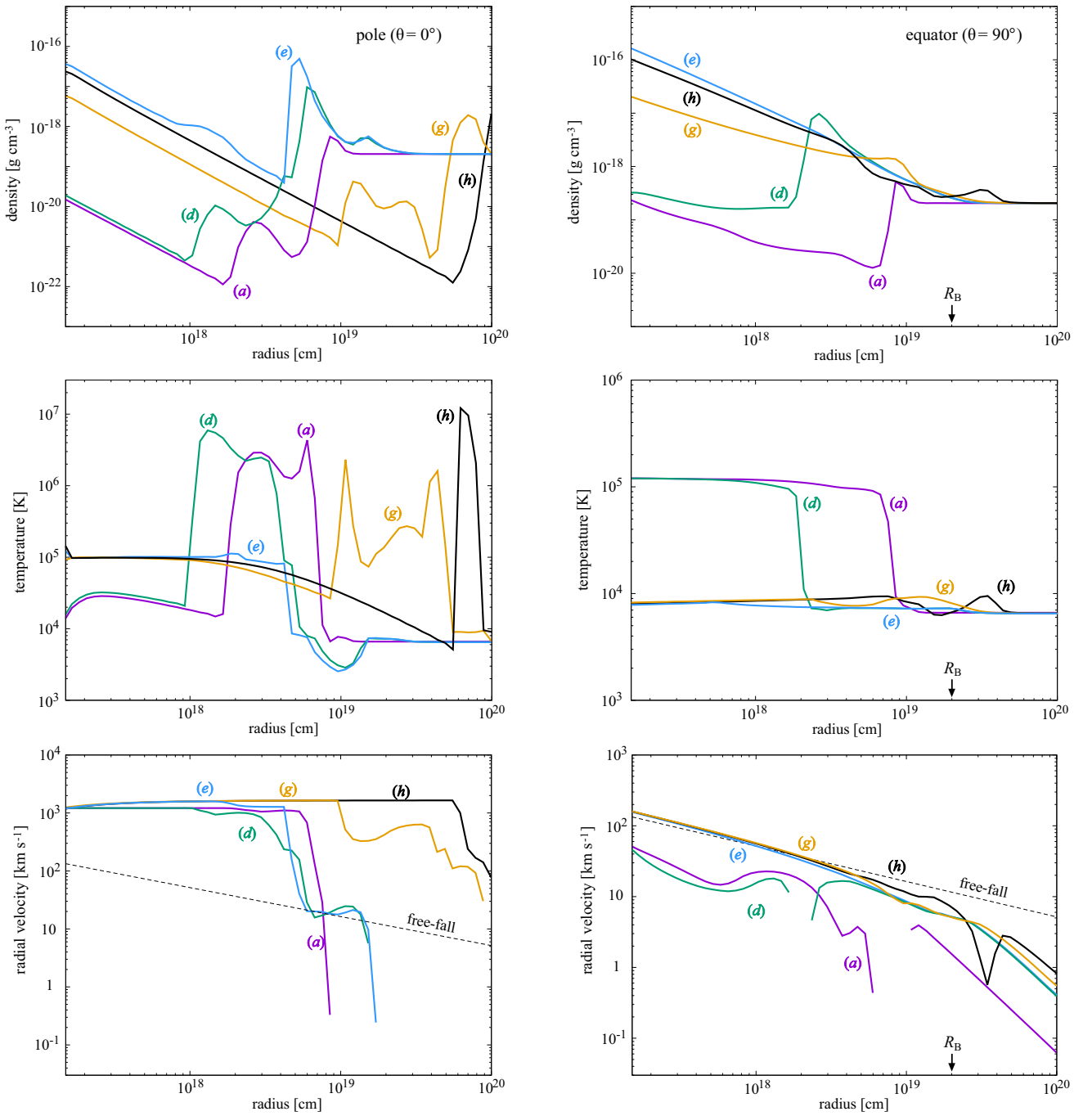


Figure 5. Radial structure of the gas density (top), temperature (middle), radial velocity (bottom) for Model A45M5 along the pole (θ = 0°; left panels) and equator (θ = 90°; right panels). In each panel, we show the profiles at different epochs during and after the transition: $t/t_{\rm dyn}$ = 0.15 (phase *a*; purple), 0.92 (phase *d*; green), 0.96 (phase *e*; blue), 1.3 (phase *g*; yellow), and 1.9 (phase *h*; black). In the bottom panels, only the outflow component along the pole and inflow component along the equator are shown. After the transition, the equatorial accretion flow settles to the isothermal Bondi solution with $T \simeq 8000$ K, whereas the outflow head continues to move outward, leading to the break out of the ambient gas cloud.

late stage (phases *d*-*h*) including the transition and rapid accretion phase.

As shown in Fig. 1, the accretion behaviour becomes less episodic after several oscillations. In the quasi-steady state ($0.3 \lesssim t/t_{\rm dyn} \lesssim 0.8$), the expansion of the ionized region halts and its size reaches a maximum value of $R_{\rm ion} \simeq 8 \times 10^{18}$ cm, which is smaller than the Bondi radius. Since ionizing radiation does not heat and prevent gas inflows from $R_{\rm B}$, neutral gas is piled up at $R_{\rm ion} \lesssim r \lesssim R_{\rm B}$ (phase *d* in Fig. 4). As the dense shell increases its mass and pushes the hot gas inwards, the ionized region gradually shrinks from the equatorial region and finally collapses (phase *e* in Fig. 4). The density cavity near the equator is totally filled by strong inflows of neutral warm gas (see phase *e* in Fig. 4 and right

panels of Fig. 5), leading to a big jump of inflow rate to $\dot{m}_{\rm in}(\equiv \dot{M}_{\rm in}/\dot{M}_{\rm Edd}) \approx 3.6\times10^3$. In the equatorial region, the accretion flow settles to an isothermal Bondi solution with $T \approx 8000$ K. On the contrary, since the intense mass inflow produces powerful outflows towards the poles, collapsing dense shell from the polar regions is blown away before reaching $r = r_{\rm min}$ (see left panels of Fig. 5).

After this abrupt transition, the inflowing region gradually becomes larger and starts to overlap with the outflowing region, suppressing mass inflows (phase *f* in Fig. 4). As the feedback strength becomes relatively weaker, a dense clump forms near the interface between the inflow and outflow region and falls into the central BH. However, since the inward ram pressure of the inflowing gas is not strong enough to overcome the momentum input by the outflow, the clump is blown away and thus the inflow rate sharply drops to $\dot{m}_{\rm in} \simeq 6\times10^2$. The episodes of clump formation and ejection are repeated but the mass inflow rate settles to a high value between $6\times10^2 \lesssim \dot{m}_{\rm in} \lesssim 2.3\times10^3$ (phase *g* in Fig. 4). As a result, the polar region is clearly evacuated and thus the central radiating source is not wholly covered by neutral gas as found in the case without mechanical feedback (Takeo et al. 2018). In the final stage of our simulation (phase *h*), the bipolar outflowing region almost totally breaks out the ambient gas cloud in the polar region. The gas temperature is shock heated up to $\sim 10^7$ K at the edge of the density cavity, and the outflow velocity is $\approx 1,000$ km s^{-1} at all radii (left panels of Fig. 5).

3.2 Effects of outflow strength and radiation anisotropy after the transition

3.2.1 Higher mass loading factor: $\beta_{\rm out} = 10$

In the above section, we set the mass loading factor to $\beta_{\rm out} = 1$ through the entire simulation. However, theoretical and numerical studies suggest that the mass loading factor could be larger than unity after the transition to hyper-Eddington accretion (see §4.2). Thus, we investigate a model with $\beta_{\rm out} = 10$ (Model A45M5-B10) to see the impact on the flow structure and differences from the fiducial model (Model A45M5; $\beta_{\rm out} = 1$).

In Fig. 6, we show the time evolution of mass inflow rates for $\beta_{\rm out} = 1$ (black) and $\beta_{\rm out} = 10$ (red). For the two cases, the time-averaged mass inflow rate is almost equivalently as high as $\dot{m}_{\rm in} \simeq 2\times10^3$, and their evolution is qualitatively similar. This clearly shows that the choice of the mass loading factor does not affect the mass inflow rate as long as outflowing matter reverses more than 50% of the inflowing matter, i.e., $\beta_{\rm out} \gtrsim 1$. One might make a misinterpretation that a higher mass loading factor leads to suppression of BH accretion because the BH accretion seems lower. However, the reduction of BH accretion rate is not caused by mechanical feedback, but is by definition of $\dot{M}_{\rm BH} = \dot{M}_{\rm in}/(1+\beta_{\rm out})$.

In Fig. 7, we present the radiative luminosity and mechanical momentum input (red and blue curves, respectively) for $\beta_{\rm out} = 1$ (solid) and $\beta_{\rm out} = 10$ (dashed), each of which is normalized by the Eddington value. Before the transition, the strength of mechanical feedback is as low as $\sim 0.01\ L_{\rm Edd}/c$, whereas the radiation luminosity is comparable to $\simeq 0.3\ L_{\rm Edd}$. This shows that gas inflow is prevented mainly by radiative feedback in the early phase. On the contrary, the power of outflows dramatically rises up to $\sim (30-100)\times L_{\rm Edd}/c$ after the transition, although the radiation luminosity is saturated at $\sim 20\ L_{\rm Edd}$ for the two cases because $L_{\rm rad}/L_{\rm Edd} \sim \ln(\dot{m}_{\rm BH})$. Thus, the flow structure is mainly determined by mechanical feedback in the later phase.

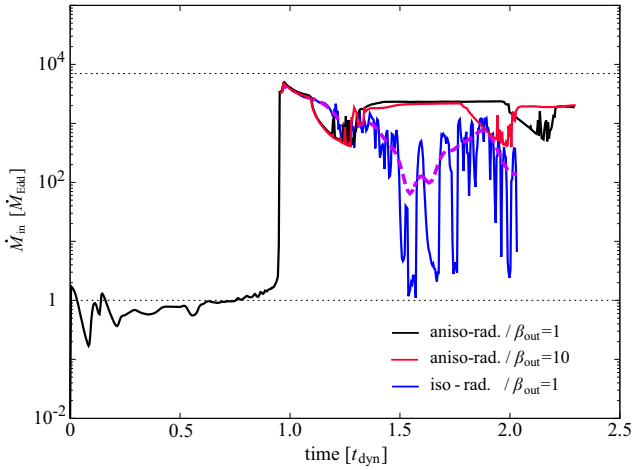


Figure 6. Time evolution of mass inflow rates $\dot{M}_{\rm in}$ for Model A45M5 (black; $\beta_{\rm out} = 1$), A45M5-B10 (blue; $\beta_{\rm out} = 10$ after the transition), and A45M5-B1-iso (blue; $\beta_{\rm out} = 1$). For Model A45M5-B1-iso, radiation field is assumed to be isotropic throughout the simulations, otherwise anisotropic radiation with an opening angle of $\theta_{\rm rad} = 45°$ is assumed after the transition. In the cases anisotropic radiation, the mass inflow rate is as high as $\dot{m}_{\rm in} \simeq 2\times10^3$, nearly independent of the mass loading factor. With isotropic radiation, the mass inflow rate is highly episodic, but the time-averaged value is $\langle \dot{m}_{\rm in} \rangle \sim 800\ \dot{M}_{\rm Edd}$ (purple).

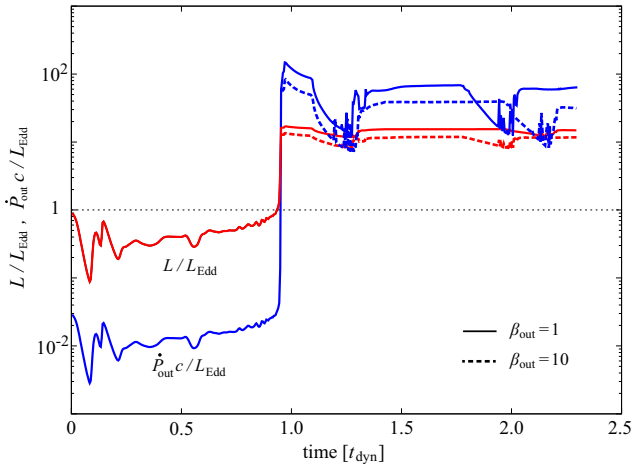


Figure 7. Time evolution of the radiative luminosity $L_{\rm rad}$ (red) and mechanical momentum input $\dot{P}_{\rm out}$ (dashed) normalized by the Eddington values for Model A45M5 (solid; $\beta_{\rm out} = 1$), and A45M5-B10 (dashed; $\beta_{\rm out} = 10$). While radiative feedback dominates before the transition, the gas dynamics after the transition is mainly determined by mechanical feedback associated with hyper-Eddington accretion.

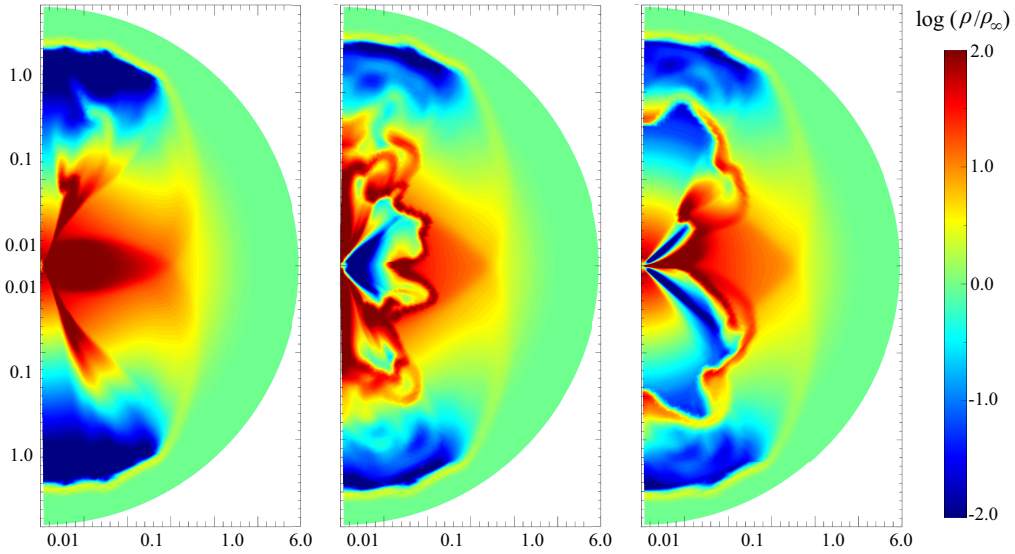


Figure 8. Two-dimensional distribution of the gas density for Model A45M5-B1-iso at different elapsed times of $t/t_{\rm dyn} = 1.20$ (left), 1.28 (middle), and 1.30 (right). Unlike the anisotropic radiation case, dense gas around the equatorial region is blown outward by radiative feedback associated with hyper-Eddington accretion at a time-averaged rate of $\dot{m}_{\rm in} \simeq 800$ (and $\dot{m}_{\rm BH} \simeq 400$).

3.2.2 Isotropic photospheric radiation field

So far, we assume radiation flux emitted from a geometrically-thick disc after the transition to be anisotropic collimated within an opening angle of $\theta_{\rm rad} = 45°$. However, radiative flux to the equatorial region is not zero but would be a significant fraction of $L_{\rm Edd}$. Presumably, the non-collimated radiation component would be emitted from the photosphere located at the outer-most disc radius or photon-trapping radius of $\sim O(10^4)\ R_{\rm Sch}$. Moreover, in such a high accretion rate, even the polar funnel regions become optically thick in the nuclear region and radiation is effectively trapped and advected towards the BH together with inflowing matter. As a result, most of the radiation energy is transported outward in the diffusion process (Jiang et al. 2019). For these reasons, we here simply assume that even after the transition, the radiation field is still isotropic with a diluted blackbody spectrum of an effective temperature of $T_{\rm eff} = (L/4\pi R_{\rm tr}^2 \sigma_{\rm SB})^{1/4}$ (Model A45M5-B1-iso), where $\sigma_{\rm SB}$ is the Stefan-Boltzmann constant and the photospheric size is approximated to be $\simeq R_{\rm tr}$, although the realistic radiation anisotropy would be somewhere between this case and previous case discussed in Section 3.1.2.

We show the time evolution of mass inflow rate (blue) and the rate averaged over a longer timescale (purple) for the isotropic radiation case in Fig. 6, and present two-dimensional distribution of the gas density after the transition in Fig. 8. Similarly to the anisotropic radiation case, high density clumps form and accrete onto the centre through the polar regions, leading to a high inflow rate of $\dot{m}_{\rm in} \sim O(10^3)$. Since radiation isotropically ionizes and heats the accreting matter, the flux preferentially propagates towards the equatorial region, where the density is relatively lower than that in the polar regions. As a result, dense gas near the equatorial region is pushed outward and thus the total mass inflow is reduced by 1-2 orders of magnitude (middle panel). Although powerful outflows evacuate the equatorial region and reduces the mass inflow rate, inflowing gas accretes again through the equatorial region with the aid of inward force exerted by positive gas pressure-gradient in the surrounding gas. Because of the symmetry breaking, the mass inflow occurs episodically but the time-averaged rate over $1.2 \leq t/t_{\rm dyn} \leq 2.0$ is $\dot{m}_{\rm in} \simeq 8.1 \times 10^2$ (see purple curve in Fig. 6).

3.3 The effects of outflow parameters on the transition

Since the outflow launching mechanisms and outflow properties are still poorly understood, we explore the dependence of the transition behaviour on the choice of model parameters; the outflow opening angle $\theta_{\rm out}$, the mass loading factor $\beta_{\rm out}$ and the outflow velocity $v_{\rm out}$ (Model A60M5 – B001M5; see Table 1). In Fig. 9, we track the time evolution of the size of the ionized region $R_{\rm ion}$ and find that the transition to rapid accretion tends to occur earlier as the outflow is stronger, i.e., larger values of $\theta_{\rm out}$, $\beta_{\rm out}$ and $v_{\rm out}$.

The reason why mechanical feedback promotes the hyper-Eddington transition is because powerful outflows reduce the BH accretion and mass inflow rate in the following ways. When the outflow is launched into a large opening angle with a higher velocity, mass inflow is allowed only through the equatorial region with a solid angle of $\Delta\Omega_{\rm in} \propto \cos\theta_{\rm out}$, otherwise strong outflows injected at the bottom reverse inflowing gas. Furthermore, a fraction $\beta_{\rm out}/(1+\beta_{\rm out})$ of the mass inflow rate is loaded into outflows, which results in a lower BH accretion rate; $\dot{M}_{\rm BH} \propto \Delta\Omega_{\rm in}/(1+\beta_{\rm out})$. Therefore, ionizing radiation attenuated by inefficient BH feeding creates a smaller ionized region that collapses within a shorter dynamical timescale as seen in Fig. 9.

Recently, Regan et al. (2019) studied the impact of bipolar jets launched from an accreting seed BH on the gas dynamics using cosmological simulations, which do not

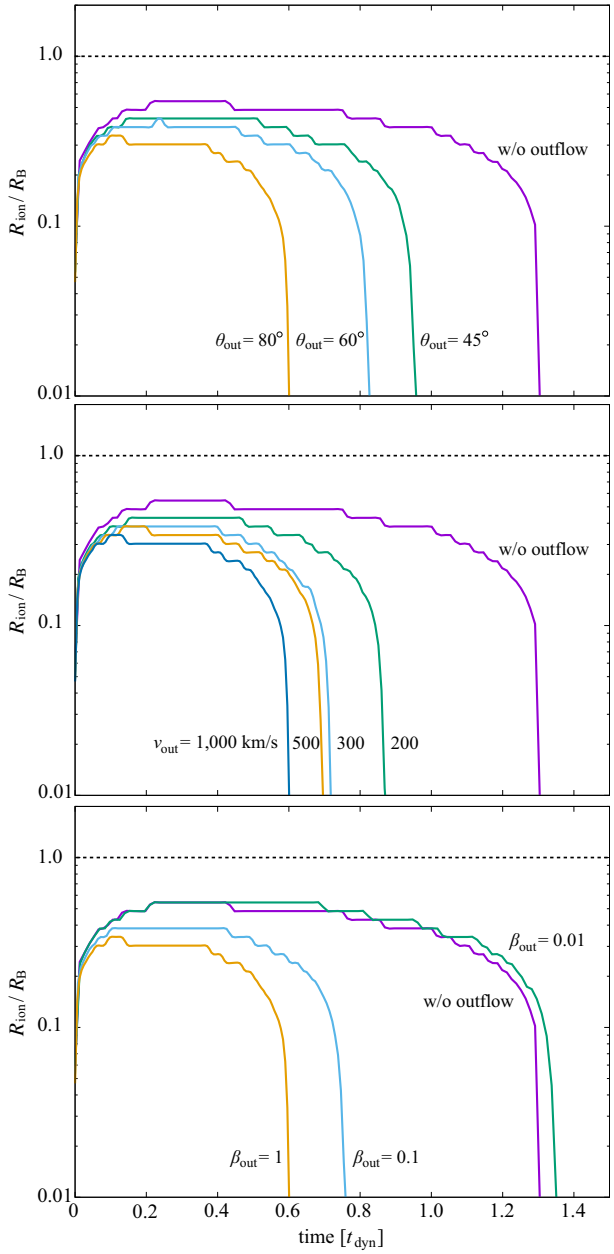


Figure 9. *Top panel*: Time evolution of the ionization radii for the cases with radiative feedback alone and with mechanical feedback injecting outflows having an opening angle of $\theta_{\rm out} = 45°$, 60° and 80°. *Middle panel*: Same as the model with $\theta_{\rm out} = 80°$ but for different outflow velocities; $v_{\rm out}$ = 200, 300, 500 and 1,000 km s^{-1}. *Bottom panel*: Same as the model with $\theta_{\rm out} = 80°$ but for different mass loading factors; $\beta_{\rm out}$ = 0.01, 0.1 and 1.0. As the outflow is stronger (i.e., a wider opening angle, higher velocity and higher mass loading factor), the transition to rapid accretion tends to occur in a shorter dynamical timescale.

consider radiative feedback due to ionizing photons. They found that the powerful jets evacuate the surrounding gas in the central ~ 0.1 pc ($\lesssim R_{\rm B}$) and lead to highly episodic mass accretion at rates ranging $10^{-3} \lesssim \dot{m}_{\rm BH} \lesssim 1$. However, their simulations do not see a transition into rapid accretion, even though neither the jets nor radiation prevents gas supply from the halo scales down to the Bondi scale. This discrepancy from our result may be because the injected feedback strength is different by orders of magnitude. In fact, they consider a constant value for the jet efficiency $\eta_{\rm jet} \sim 0.64$ [$\equiv L_{\rm out}/(\dot{M}_{\rm BH}c^2)$], assuming that the innermost disc can be a magnetically arrested disc (Tchekhovskoy et al. 2011), where the jet efficiency depends on the BH spin $a_{\rm BH}$ and can be described as $\eta_{\rm jet} \simeq 1.3\, a_{\rm BH}^2$ (Tchekhovskoy 2015). Since the jet efficiency is rewritten as $\eta_{\rm jet} = 0.5\beta_{\rm out}(v_{\rm out}/c)^2$, the mass-loading factor adopted in Regan et al. (2019) is as high as $\beta_{\rm out} \simeq 100$ (10^4) for $v_{\rm out} = 0.1c$ ($0.01c$). Such a high mass loading factor leads to a significant reduction of BH accretion rate, i.e., $\dot{M}_{\rm BH} \sim \dot{M}_{\rm in}/(1+\beta_{\rm out})$, and limit the rate below the Eddington value even if the mass inflow rate is a super/hyper-Eddington value independent of $\beta_{\rm out}$ (see also discussion in 3.2.1 and Fig. 6).

4 DISCUSSION

4.1 Revised transition criterion

In our previous studies, we quantify the conditions required for the transition to rapid accretion only when the accreting gas is exposed to ionizing radiation associated with BH feeding (Inayoshi et al. 2016; Takeo et al. 2018, 2019), where the conditions are characterized by the dimensionless Bondi accretion rate[2]; $\dot{M}_{\rm B}/\dot{M}_{\rm Edd} \gtrsim 500$. We here extend this criterion for the transition to the case with mechanical feedback. In Fig. 10, we summarize the results for two different BH masses of $M_{\rm BH} = 10$ and 10^5 M$_\odot$ with several different values of n_∞, where the outflow model parameters are set to $\theta_{\rm out} = 80°$, $\beta_{\rm out} = 1$, and $v_{\rm out} = 1,000$ km s^{-1} (Model T34M5 – T17M1; see Table 1). In order to save the computation time, we adopt $\theta_{\rm out} = 80°$ because the transition, if any, occurs in a shorter timescale (see discussion in §3.3). For each BH mass, the transition to hyper-Eddington accretion is found in cases with higher ambient gas density (blue circles), while the transition is not seen in cases with lower density within $\sim 5\ t_{\rm dyn}$ (orange circles). The red shaded region marks the boundary between the two accretion modes under mechanical feedback. We also overlay the critical conditions obtained by 1D RHD simulations (Inayoshi et al. 2016, black line) and 2D RHD simulations with power-law spectra and disc multi-colour blackbody spectra (green and blue region, respectively; Takeo et al. 2019). The results show that mechanical feedback reduces the critical density by a factor of $\simeq 2-4$ nearly independently of BH mass.

The critical conditions for the hyper-Eddington transition is evaluated in the following analytical argument, comparing the Bondi radius and the ionization radius (Inayoshi et al. 2016). We approximate the size of ionized regions by the Strömgren radius, where the number flux of ionizing photons for disc radiation spectra is estimated as

$$\dot{N}_{\rm ion} = \int_{\nu_{\rm min}}^{\nu_{\rm cut}} {\rm d}\nu\ \frac{L_\nu}{h\nu} \approx 2\times10^{46}\ {\rm s}^{-1}\ M_{\rm BH}^{1.3}\ \dot{m}_{\rm BH}^{0.75}, \tag{28}$$

where the above expression is valid at $1 < M_{\rm BH}/{\rm M}_\odot < 10^6$ and $10^{-2} < \dot{m}_{\rm BH} < 10$. We note that the cutoff frequency

[2] The exact value of critical rate depends on the radiation spectral model and has a scaling relation of $\propto \langle h\nu\rangle^{-5/9}$, where $\langle h\nu\rangle$ is the mean energy of ionizing radiation (Takeo et al. 2019).

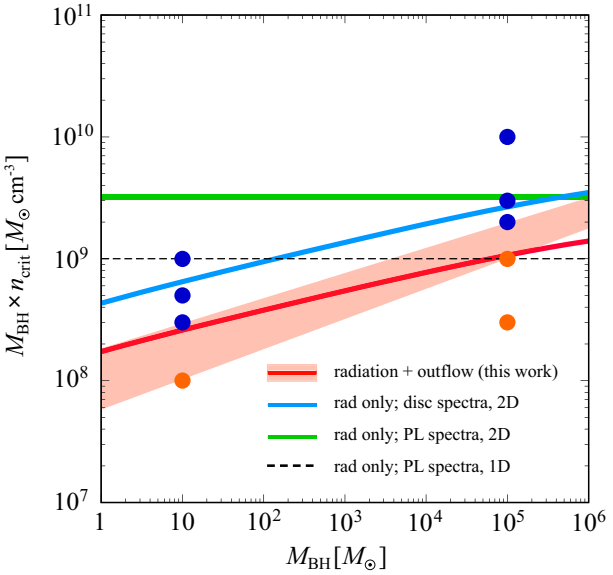


Figure 10. Summary of our simulation results for $M_{\rm BH}$ = 10 and 10^5 $M_\odot$. The outflow opening angle is set to $\theta_{\rm out} = 80°$, the mass loading factor is $\beta_{\rm out} = 1$, and the outflow velocity is $v_{\rm out} = 1,000$ km s^{-1}. Each symbol indicates whether the final result is hyper-Eddington accretion (blue circle), or episodic accretion at the rate of $\lesssim \dot{M}_{\rm Edd}$ (orange circle). The red shaded region marks the boundary between the two accretion modes obtained from the simulation data. Each solid curve shows the transition criterion derived by the analytical argument in §4.1 that takes into account both radiative and mechanical feedback (red; see Eq. 32), radiative feedback alone assuming disc spectra (blue) and power-law spectra (green), respectively. The critical density required for hyper-Eddington accretion with outflows is reduced by a factor of $\sim 2-4$ from that with radiative feedback alone nearly independent of BH mass, and is also lower than 1D simulations estimated (dashed line Inayoshi et al. 2016).

for the integration is set to $h\nu_{\rm cut} = 100$ eV, because higher-energy photons hardly ionize gas[3]. Using the expression and setting $\dot{m}_{\rm BH} = 1$, the ratio of $R_{\rm ion}/R_{\rm B}$ before the transition is evaluated as

$$\frac{R_{\rm ion}}{R_{\rm B}} \propto \dot{N}_{\rm ion}^{1/3} n_\infty^{-2/3} M_{\rm BH}^{-1} \propto M_{\rm BH}^{(\alpha-3)/3} n_\infty^{-2/3}, \quad (29)$$

where $\dot{N}_{\rm ion} \propto M_{\rm BH}^{\alpha}$ ($\alpha = 1.3$ in Eq. 28 and $\alpha = 1$ for power-law spectra). By equating $R_{\rm ion} \simeq R_{\rm B}$, we obtain the critical density for the transition as

$$n_{\rm crit} \propto M_{\rm BH}^{-1+(\alpha-1)/2}. \quad (30)$$

Therefore, the critical condition is given by $M_{\rm BH} \times n_{\rm crit} \propto M_{\rm BH}^{0.15}$ (blue curve in Fig. 10) for disc spectra at $1 < M_{\rm BH}/{\rm M}_\odot < 10^6$ ($M_{\rm BH} \times n_{\rm crit} = $ const. for power-law spectra; see green and black lines in Fig. 10). The lower critical density reflects that the radiation spectrum for lower BH mass is so hard that a significant fraction of photons do not contribute to ionization.

[3] Takeo et al. (2019) do not set the cutoff, namely $\nu_{\rm cut} \to \infty$. Therefore, $N_{\rm ion}$ is overestimated and the BH mass dependence is modest. In fact, the numerical result obtained in Takeo et al. (2019) is nicely explained by the evaluation of $\dot{N}_{\rm ion}$ in Eq. (28).

With mechanical feedback, the estimate of $\dot{N}_{\rm ion}$ is modified as follows. As the outflow opening angle is wider and mass loading factor is higher, the BH accretion rate and radiation luminosity decrease. We approximate the ionizing photon number flux as $\dot{N}_{\rm ion} \propto \dot{m}_{\rm BH}^{3/4} \propto [\Delta\Omega_{\rm in}/(1+\beta_{\rm out})]^{3/4}$ (see discussion §3.3). Therefore, the size of ionized region is evaluated as

$$R_{\rm ion} \propto \left[\frac{\cos\theta_{\rm out}}{(1+\beta_{\rm out})}\right]^{1/4} n_\infty^{-2/3}, \quad (31)$$

where the part of [...] is a correction factor from the mechanical feedback effect. By equating $R_{\rm ion} \simeq R_{\rm B}$, we obtain the critical density with mechanical feedback as

$$n_{\rm crit,mf} \simeq \left[\frac{\cos\theta_{\rm out}}{(1+\beta_{\rm out})}\right]^{3/8} n_{\rm crit} \equiv \mathcal{F} n_{\rm crit}. \quad (32)$$

For $\theta_{\rm out} = 80°$ and $\beta_{\rm out} = 1$, the correction factor is $\mathcal{F} \simeq 0.4$, and the critical density is given as $n_{\rm crit,mf} \simeq 1.2 \times 10^4$ cm^{-3} (2.5×10^7 cm^{-3}) for $M_{\rm BH} = 10^5$ $M_\odot$ (10 $M_\odot$), which nicely agrees to the simulation result (red curve in Fig. 10).

We note that in the analytical argument above, we implicitly assume $\dot{M}_{\rm BH} \propto \Delta\Omega_{\rm in}$. In fact, the simulation result indicates a modest $\Delta\Omega_{\rm in}$-dependence. This is because gas in the equatorial region is compressed owing to expansion of the outflow region in the tangential direction and the density of inflowing gas through the equator increases. As the level of compression increases with the outflow opening angle, the dependence of $\dot{M}_{\rm BH}$ on $\Delta\Omega_{\rm in}$ becomes weaker than the linear relation. However, gas compression makes radiative recombination more efficient simultaneously, and promotes collapse of the ionized region. As a result, our estimation assuming Eq. (32) nicely agrees with our numerical results, although the compressional degree at the different radii is not modelled analytically.

4.2 Typical outflow parameters

In our study, we investigate the impact of mechanical feedback on BH accretion, assuming the mass-loading factor and velocity at the injection scale. We briefly summarize the outflow properties expected from recent numerical studies and discuss the uncertainties of the outflow model parameters.

As discussed in §4.1, the BH accretion rate is limited to $\dot{m}_{\rm BH} \lesssim 1$ before the transition. In the sub-Eddington accretion phase, strong mass loss would be driven from the nuclear accretion disc scale via several different mechanisms. A widely accepted idea is that the large scale magnetic field with poloidal topology plays a key role in acceleration and collimation of outflows and/or jets (e.g., Blandford & Znajek 1977; Blandford & Payne 1982). Depending on the configuration and strength of magnetic field, there is a wide range of predictions for the properties of outflows (e.g., Jafari 2019, and references therein). With a semi-analytical model of a sub-Eddington disc, Li & Cao (2019) find that strong mass loss driven by large-scale poloidal magnetic fields accumulated near the BH with accretion injects matter into outflows with a mass loading factor of $\beta_{\rm out} \approx 0.3-2$ (a higher $\beta_{\rm out}$ with stronger magnetic field). The outflow velocity reaches $\simeq 0.1-0.2\,c$ in the inner region and decreases outward. In fact, a significant mass fraction of the outflow ($\gtrsim 50-70$ %) has a relatively low velocity of $< 0.01\,c$, which is comparable to that in our fiducial value of $v_{\rm out} = 1,000$ km s^{-1}.

Even in the sub-Eddington regime, radiation emitted from the nuclear disc can contribute to the acceleration of outflows by the line force due to bound-free absorption. The line force increases by several orders of magnitude above the continuum radiation force exerted through electron scattering alone, leading to high-speed outflows at $\simeq 0.05-0.1\ c$ (Proga et al. 2000; Proga & Kallman 2004). A recent numerical study by Nomura et al. (2018) found that the mass loading factor is as high as $\beta_{\rm out} \lesssim 1.2$ when the mass inflow rate from larger radii is $0.3 \lesssim \dot{m}_{\rm in} \lesssim 1.5$. In addition, X-ray emission from the inner disc and/or corona heats the surface of the disc at larger radii up to the Compton temperature (e.g., Begelman et al. 1983; Done et al. 2018). The heated gas becomes unbound at the outer part of the disc and produces thermal-driven outflows with a mass loading factor of $\beta_{\rm out} \sim O(1)$ at a terminal velocity of $v_{\rm out} \simeq 300-1,000$ km s^{-1}, which is the order of the sound speed of X-ray irradiated gas.

In the hyper-Eddington accretion phase after the transition, radiation force through electron scattering in optically-thick medium produces strong mass outflows from the accretion disc. Numerical simulation studies suggested that the mass loading factor in the radiation-driven outflow is as high as $\beta_{\rm out} \sim 0.05-0.3$ for $\dot{m}_{\rm BH} \sim 5-20$ (Ohsuga et al. 2009; Ohsuga & Mineshige 2014; Jiang et al. 2019). As the accretion rate rises, the value of $\beta_{\rm out}$ gradually increases; namely $\beta_{\rm out} \simeq 6-7$ for $\dot{m}_{\rm BH} \approx 10^2$ (Kawashima et al. 2009). The outflow velocity is accelerated up to $\sim 0.2-0.5\ c$ for $10 \lesssim \dot{m}_{\rm BH} \lesssim 10^2$ (Ohsuga et al. 2009; Kawashima et al. 2009).

In summary, the mass loading factor obtained from numerical and semi-analytical studies is $\beta_{\rm out} \sim 1$ and $\beta_{\rm out} \lesssim 10$ before and after the transition, respectively. Depending on the outflow launching mechanisms and accretion rates, the outflow velocity would be accelerated to several percent of light speed, which is commonly observed in luminous AGNs (Tombesi et al. 2010, 2011). Since the typical velocity of outflows tends to higher than our fiducial value by one order of magnitude, our result seems conservative for determining the criteria required for the hyper-Eddington transition (see in §3.3).

4.3 Impact of BH feedback on the host galaxy evolution

Rapid assembly of massive black holes via gas accretion is a key ingredient to understand the formation of high-z SMBHs, which would require super/hyper-Eddington accretion but with a low duty cycle. In a cosmological context, the rapid accretion mode would invoke the rapid collapse of chemically pristine primordial gas in so-called "atomic cooling halos" with virial temperature of $T_{\rm vir} \sim 10^4$ K (Volonteri & Rees 2005; Inayoshi et al. 2016; Pezzulli et al. 2016), where a dense core region is developed at the nuclei of protogalaxies that do not experience prior star formation (Wise et al. 2008; Regan et al. 2014). In recent decades, both semi-analytical models and cosmological simulations have been utilized to study the coevolution of SMBHs with their host galaxies, including various feedback processes associated with supernovae and AGN activity. Due to numerical limitations (e.g., spatial resolutions), however, a great number of studies treat feedback effects using sub-grid models instead of directly resolving physical processes within the Bondi scales. In addition to feedback mechanisms, most cosmological simulations calculate the feeding rate onto unresolved BHs, assuming $\dot{M}_{\rm BH} = \min(\dot{M}_{\rm B},\ \dot{M}_{\rm Edd})$ without permitting super/hyper-Eddington accretion. Therefore, the link between the model and physical processes of mass accretion and ejection from the nuclear region is still highly uncertain.

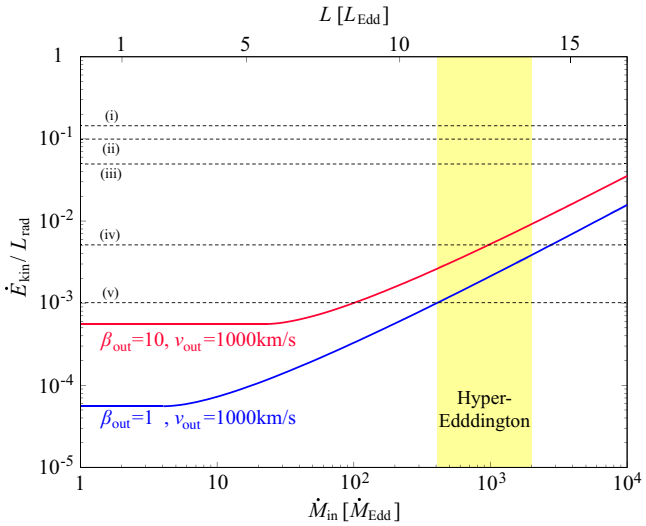


Figure 11. Kinetic coupling efficiency ($\dot{E}_{\rm out}/L_{\rm rad}$) in our feedback model for hyper-Eddington accretion as a function of mass inflow rate $\dot{M}_{\rm in}$; Model A45M5 ($\beta_{\rm out}$ = 1; blue) and A45M5-B10 ($\beta_{\rm out}$ = 10; red). The upper horizontal axis shows the radiative luminosity (in units of $L_{\rm Edd}$) for $\beta_{\rm out}$ = 1. The yellow shaded region presents the mass inflow rates for hyper-Eddington accretion phases accompanied by powerful outflows. Theoretical values adopted in cosmological simulations as sub-grid parameters are shown by horizontal lines: from the top to the bottom (i) Dubois et al. (2014); Schaye et al. (2015), (ii) Weinberger et al. (2017), (iii) Di Matteo et al. (2005), (iv) Hopkins & Elvis (2010), and (v) Costa et al. (2018).

In studies of AGN feedback both observationally and theoretically, the kinetic coupling efficiency defined by the ratio of the kinetic luminosity of outflows to the AGN radiative luminosity, $\dot{E}_{\rm out}/L_{\rm rad}$, is often used to characterize the AGN outflow properties (Harrison et al. 2018, reference therein). In Fig. 11, we show the kinetic coupling efficiency calculated with the feedback model discussed in §2 for two different outflow parameters (solid curves). In the limit of high accretion rates ($\dot{m}_{\rm BH} \gg 1$), the value can be approximated as

$$\frac{\dot{E}_{\rm out}}{L_{\rm rad}} \simeq \frac{5}{2}\beta_{\rm out}\ \frac{\dot{m}_{\rm BH}}{\ln(\dot{m}_{\rm BH}/2)}\left(\frac{v_{\rm out}}{c}\right)^2, \tag{33}$$

where $\dot{m}_{\rm BH} = \dot{m}_{\rm in}/(1+\beta_{\rm out})$. This relation weakly depends on the mass loading factor but strongly depends on the outflow velocity. Since the range of mass inflow rates obtained from Model A45M5 ($\beta_{\rm out}$ = 1; blue) and A45M5-B10 ($\beta_{\rm out}$ = 10; red) is $400 < \dot{m}_{\rm in} < 2000$ in their hyper-Eddington stages, the kinetic coupling efficiency is $\sim 0.1-1\%$ of the radiative luminosity. We also overlay representative values for the kinetic coupling efficiencies adopted in cosmological simulations as sub-grid parameters, ranging $\sim 0.1-10\%$ of the radiative luminosity: from the top to the bottom (i) Dubois et al. (2014); Schaye et al. (2015), (ii) Weinberger

et al. (2017), (iii) Di Matteo et al. (2005), (iv) Hopkins & Elvis (2010), and (v) Costa et al. (2018). Although the fiducial values in our model are located at the lower end, the mechanical power associated with highly accreting massive BHs, $\dot{E}_{\rm out}/L_{\rm rad} \simeq 10^{-3} - 10^{-2}$, would impact upon their host galaxies with a significant delay time, which might be marginally longer than the typical AGN lifetime (e.g., Costa et al. 2018). Finally, we note that the expression of Eq. (33) can be applied *only when the transition criterion for hyper-Eddington accretion is satisfied, i.e., a mass inflow rate exceeding* $\simeq 300\ \dot{M}_{\rm Edd}$ *is found at the inner-most cells large-scale cosmological simulations.*

5 SUMMARY

We investigate the properties of accretion flows onto BHs at the nuclei of protogalaxies and study the impact of mechanical and radiative feedback on rapid growth of BHs, performing two-dimensional RHD simulations that take into account mechanical feedback with a phenomenological outflow model. In our fiducial case ($\theta_{\rm out} = 45^\circ$, $\beta_{\rm out} = 1$, and $v_{\rm out} = 1,000$ km s^{-1}), we find that the flow structure consists of two distinct parts before the transition; the bipolar outflowing region heated up to $T \sim 10^{6-7}$ K due to strong shock and the equatorial inflowing region where ionized gas is mildly heated to $T \sim 10^5$ K due to photoionization. Since the outflows inject momentum and energy into the surrounding medium and prevent mass accretion onto the BH, radiative output from the accreting BH is reduced. When the BH is embedded in a dense gas core, attenuated ionizing radiation hardly affects the gas dynamics at the Bondi radius, from which intense inflows of neutral gas occur at rates substantially exceeding the Eddington limit without impeded by photoionization and heating. After the transition to the hyper-Eddington accretion phase, strong bipolar outflows completely evacuate the surrounding gas in the polar region but mass inflows through the equatorial region maintain the BH accretion rate as high as $\sim 300 - 10^3\ \dot{M}_{\rm Edd}$, which is reduced by one order of magnitude from those with radiative feedback alone. We note the mass inflow rate and flow structure in the rapidly accreting stage barely depend on the mass loading factor into outflows, while more spherical radiation field makes the mass inflow highly episodic (the time-averaged accretion rate does not change significantly).

In order to derive the necessary conditions required for the transition, we conduct a comprehensive survey on the model parameter dependence, varying the outflow opening angle, mass-loading factor, outflow velocity, and density of gas surrounding the BH. We find that the critical density above which the transition occurs is reduced by a factor of ~ 3, nearly independently of BH mass, when mechanical feedback is considered. We also conclude that contrary to naive expectation, the existence of stronger outflow (i.e., a wider opening angle, higher mass-loading factor, and higher outflow velocity) leads to the transition to rapid accretion phases more efficiently. This is because the suppression of BH accretion owing to outflows reduces the radiative output from the nuclear BH, making a smaller ionized region surrounding the BH that collapse in a shorter dynamical timescale.

Finally, we discuss the application of our result as a sub-grid model for cosmological simulations that do not directly resolve the nuclear region scale. Rapidly growing BHs inject mechanical power with $\sim 0.1-1\%$ of the radiative luminosity (see Eq. 33) and would impact on their host galaxies.

ACKNOWLEDGEMENTS

We would like to thank Ken Ohsuga and Hiroyuki R. Takahashi for providing their numerical code and discussions. We also thank Kazuyuki Sugimura and Ryota Tomaru for fruitful discussion. This work is partially supported by the National Science Foundation of China (11721303, 11991052, 11950410493), the National Key R&D Program of China (2016YFA0400702), and by JSPS Grant-in-Aid for Scientific Research (C) (17K0583 SM). Numerical computations were carried out on Cray XC50 at Center for Computational Astrophysics, National Astronomical Observatory of Japan, and High-performance Computing Platform of Peking University.

REFERENCES

Abel T., Anninos P., Zhang Y., Norman M. L., 1997, New Astron., 2, 181
Abramowicz M. A., Czerny B., Lasota J. P., Szuszkiewicz E., 1988, ApJ, 332, 646
Alvarez M. A., Wise J. H., Abel T., 2009, ApJ, 701, L133
Bañados E., et al., 2018, Nature, 553, 473
Begelman M. C., McKee C. F., Shields G. A., 1983, ApJ, 271, 70
Blandford R. D., Payne D. G., 1982, MNRAS, 199, 883
Blandford R. D., Znajek R. L., 1977, MNRAS, 179, 433
Bondi H., 1952, MNRAS, 112, 195
Bromm V., Loeb A., 2003, ApJ, 596, 34
Choi E., Ostriker J. P., Naab T., Johansson P. H., 2012, ApJ, 754, 125
Chon S., Omukai K., 2020, arXiv e-prints, p. arXiv:2001.06491
Ciotti L., Ostriker J. P., 2001, ApJ, 551, 131
Ciotti L., Pellegrini S., Negri A., Ostriker J. P., 2017, ApJ, 835, 15
Costa T., Rosdahl J., Sijacki D., Haehnelt M. G., 2018, MNRAS, 473, 4197
Devecchi B., Volonteri M., 2009, ApJ, 694, 302
Di Matteo T., Springel V., Hernquist L., 2005, Nature, 433, 604
Dijkstra M., Haiman Z., Mesinger A., Wyithe J. S. B., 2008, MNRAS, 391, 1961
Done C., Tomaru R., Takahashi T., 2018, MNRAS, 473, 838
Dubois Y., Devriendt J., Slyz A., Teyssier R., 2010, MNRAS, 409, 985
Dubois Y., et al., 2014, MNRAS, 444, 1453
Fan X., et al., 2004, AJ, 128, 515
Glover S. C. O., Jappsen A.-K., 2007, ApJ, 666, 1
Haiman Z., 2013, in Wiklind T., Mobasher B., Bromm V., eds, Astrophysics and Space Science Library Vol. 396, Astrophysics and Space Science Library. p. 293 (arXiv:1203.6075), doi:10.1007/978-3-642-32362-1_6
Harrison C. M., Costa T., Tadhunter C. N., Flütsch A., Kakkad D., Perna M., Vietri G., 2018, Nature Astronomy, 2, 198
Harten A., Lax P. D., van Leer B., 1983, SIAM Review, 25, 35
Hopkins P. F., Elvis M., 2010, MNRAS, 401, 7
Inayoshi K., Omukai K., Tasker E., 2014, MNRAS, 445, L109
Inayoshi K., Haiman Z., Ostriker J. P., 2016, MNRAS, 459, 3738
Inayoshi K., Li M., Haiman Z., 2018, MNRAS, 479, 4017
Inayoshi K., Visbal E., Haiman Z., 2019, arXiv e-prints, p. arXiv:1911.05791

Jafari A., 2019, arXiv e-prints, p. arXiv:1904.09677
Jeon M., Pawlik A. H., Greif T. H., Glover S. C. O., Bromm V., Milosavljević M., Klessen R. S., 2012, ApJ, 754, 34
Jiang Y.-F., Stone J. M., Davis S. W., 2014, ApJ, 796, 106
Jiang Y.-F., Stone J. M., Davis S. W., 2019, ApJ, 880, 67
Johnson J. L., Dalla Vecchia C., Khochfar S., 2013, MNRAS, 428, 1857
Kato Y., Mineshige S., Shibata K., 2004, ApJ, 605, 307
Kato S., Fukue J., Mineshige S., 2008, Black-Hole Accretion Disks — Towards a New Paradigm —. Kyoto University Press
Kawashima T., Ohsuga K., Mineshige S., Heinzeller D., Takabe H., Matsumoto R., 2009, PASJ, 61, 769
King A., 2003, ApJ, 596, L27
King A. R., Davies M. B., Ward M. J., Fabbiano G., Elvis M., 2001, ApJ, 552, L109
Kormendy J., Ho L. C., 2013, ARA&A, 51, 511
Latif M. A., Schleicher D. R. G., Hartwig T., 2016, MNRAS, 458, 233
Li J., Cao X., 2019, ApJ, 872, 149
Matsuoka Y., et al., 2018a, PASJ, 70, S35
Matsuoka Y., et al., 2018b, ApJS, 237, 5
Matsuoka Y., et al., 2018c, ApJ, 869, 150
McKinney J. C., Tchekhovskoy A., Sadowski A., Narayan R., 2014, MNRAS, 441, 3177
Milosavljević M., Couch S. M., Bromm V., 2009a, ApJ, 696, L146
Milosavljević M., Bromm V., Couch S. M., Oh S. P., 2009b, ApJ, 698, 766
Mineshige S., Kawaguchi T., Takeuchi M., Hayashida K., 2000, PASJ, 52, 499
Mortlock D. J., et al., 2011, Nature, 474, 616
Murray N., Quataert E., Thompson T. A., 2005, ApJ, 618, 569
Nomura M., Ohsuga K., Takahashi H. R., Wada K., Yoshida T., 2016, PASJ, 68, 16
Nomura M., Ohsuga K., Done C., 2018, arXiv e-prints, p. arXiv:1811.01966
Novak G. S., Ostriker J. P., Ciotti L., 2011, ApJ, 737, 26
Ohsuga K., Mineshige S., 2011, ApJ, 736, 2
Ohsuga K., Mineshige S., 2014, Space Sci. Rev., 183, 353
Ohsuga K., Mori M., Nakamoto T., Mineshige S., 2005, ApJ, 628, 368
Ohsuga K., Mineshige S., Mori M., Kato Y., 2009, PASJ, 61, L7
Onoue M., et al., 2019, arXiv e-prints, p. arXiv:1904.07278
Ostriker J. P., Choi E., Ciotti L., Novak G. S., Proga D., 2010, ApJ, 722, 642
Park K., Ricotti M., 2011, ApJ, 739, 2
Park K., Ricotti M., 2012, ApJ, 747, 9
Pezzulli E., Valiante R., Schneider R., 2016, MNRAS, 458, 3047
Proga D., Kallman T. R., 2004, ApJ, 616, 688
Proga D., Stone J. M., Kallman T. R., 2000, ApJ, 543, 686
Qiu Y., Bogdanović T., Li Y., Park K., Wise J. H., 2019, ApJ, 877, 47
Regan J. A., Johansson P. H., Haehnelt M. G., 2014, MNRAS, 439, 1160
Regan J. A., Downes T. P., Volonteri M., Beckmann R., Lupi A., Trebitsch M., Dubois Y., 2019, MNRAS, 486, 3892
Ricotti M., Gnedin N. Y., Shull J. M., 2002, ApJ, 575, 33
Sądowski A., Narayan R., Tchekhovskoy A., Abarca D., Zhu Y., McKinney J. C., 2015, MNRAS, 447, 49
Schaye J., et al., 2015, MNRAS, 446, 521
Shakura N. I., Sunyaev R. A., 1973, A&A, 24, 337
Shang C., Bryan G. L., Haiman Z., 2010, MNRAS, 402, 1249
Shull J. M., van Steenberg M. E., 1985, ApJ, 298, 268
Silk J., Rees M. J., 1998, A&A, 331, L1
Sugimura K., Omukai K., Inoue A. K., 2014, MNRAS, 445, 544
Sugimura K., Hosokawa T., Yajima H., Omukai K., 2017, MNRAS, 469, 62
Tagawa H., Haiman Z., Kocsis B., 2019, arXiv e-prints, p. arXiv:1909.10517
Takahashi H. R., Ohsuga K., 2013, ApJ, 772, 127
Takahashi H. R., Ohsuga K., Kawashima T., Sekiguchi Y., 2016, ApJ, 826, 23
Takeo E., Inayoshi K., Ohsuga K., Takahashi H. R., Mineshige S., 2018, MNRAS, 476, 673
Takeo E., Inayoshi K., Ohsuga K., Takahashi H. R., Mineshige S., 2019, MNRAS, 488, 2689
Tanaka T., Haiman Z., 2009, ApJ, 696, 1798
Tanaka T. L., Li M., 2014, MNRAS, 439, 1092
Tchekhovskoy A., 2015, Launching of Active Galactic Nuclei Jets. p. 45, doi:10.1007/978-3-319-10356-3_3
Tchekhovskoy A., Narayan R., McKinney J. C., 2011, MNRAS, 418, L79
Tombesi F., Cappi M., Reeves J. N., Palumbo G. G. C., Yaqoob T., Braito V., Dadina M., 2010, A&A, 521, A57
Tombesi F., Cappi M., Reeves J. N., Palumbo G. G. C., Braito V., Dadina M., 2011, ApJ, 742, 44
Toyouchi D., Hosokawa T., Sugimura K., Nakatani R., Kuiper R., 2019, MNRAS, 483, 2031
Visbal E., Haiman Z., Bryan G. L., 2014, MNRAS, 445, 1056
Volonteri M., 2012, Science, 337, 544
Volonteri M., Rees M. J., 2005, ApJ, 633, 624
Wang J.-M., Szuszkiewicz E., Lu F.-J., Zhou Y.-Y., 1999, ApJ, 522, 839
Watarai K.-y., 2006, ApJ, 648, 523
Watarai K.-y., Fukue J., Takeuchi M., Mineshige S., 2000, PASJ, 52, 133
Watarai K.-y., Mizuno T., Mineshige S., 2001, ApJ, 549, L77
Weinberger R., et al., 2017, MNRAS, 465, 3291
Whalen D., Norman M. L., 2006, ApJS, 162, 281
Wise J. H., Turk M. J., Abel T., 2008, ApJ, 682, 745
Wise J. H., Regan J. A., O'Shea B. W., Norman M. L., Downes T. P., Xu H., 2019, Nature, 566, 85
Wolcott-Green J., Haiman Z., Bryan G. L., 2017, MNRAS, 469, 3329
Wu X.-B., et al., 2015, Nature, 518, 512
Yajima H., Ricotti M., Park K., Sugimura K., 2017, ApJ, 846, 3
Yuan F., Yoon D., Li Y.-P., Gan Z.-M., Ho L. C., Guo F., 2018, ApJ, 857, 121
van Leer B., 1977, Journal of Computational Physics, 23, 263

This paper has been typeset from a TEX/LATEX file prepared by the author.